Linearly Ordered Pt_2Rh and Pt_2Ir Heterotrinuclear Complexes Bridged by Tridentate Phosphine Ligands

Tomoaki Tanase,*,† Rowshan Ara Begum,† Hirotaka Toda,‡ and Yasuhiro Yamamoto‡

Department of Chemistry, Faculty of Science, Nara Women's University, Kitauoya-higashi-machi, Nara 630-8285, Japan, and Department of Chemistry, Faculty of Science, Toho University, Miyama 2-2-1, Funabashi, Chiba 274-8510, Japan

Received October 2, 2000

Reactions of the diplatinum complex supported by two tridentate phosphine ligands, *syn*-$[Pt_2(\mu\text{-dpmp})_2L_2](PF_6)_2$ (**1**), with $[MCl(cod)]_2$ (M = Rh, Ir) afforded the linearly ordered Pt−Pt−M clusters $[Pt_2\{MClL\}(\mu\text{-dpmp})_2L](PF_6)_2$ (**6a**, M = Rh; **6b**, M = Ir) and the asymmetrical A-frame clusters $[Pt_2\{M(\mu\text{-Cl})L\}(\mu\text{-dpmp})_2L](PF_6)_2$ (**7a**, M = Rh; **7b**, M = Ir), where dpmp = bis(diphenylphosphinomethyl)phenyphosphine and L = 2,6-xylyl isocyanide (XylNC). Complexes **6** involve a linear Pt_2M trinuclear core supported by two dpmp ligands. The three metals are joined by two metal−metal bonds, where the Pt−Pt and Pt−M bonds can be viewed, respectively, as a d^9−d^9 covalent and a d^9←d^8 dative interactions. Complexes **7** consists of an asymmetrical $Pt_2(\mu\text{-Cl})M$ A-frame structure. Reaction of **6a** with 1 equiv of L (= XylNC) yielded $[Pt_2\{RhClL_2\}(\mu\text{-dpmp})_2L](PF_6)_2$ (**8a**), and that with excess L led to $[Pt_2\{RhL_3\}(\mu\text{-dpmp})_2L](PF_6)_3$ (**9a**). The additional isocyanide molecules are attached exclusively to the Rh center. Complex **6a** by treatment with CO was readily converted into an CO adduct, $[Pt_2\{RhClL(\mu\text{-CO})\}(\mu\text{-dpmp})_2L](PF_6)_2$ (**10a**), which easily regenerated **6a** with dinitrogen passed through its solution. The structure of **10a** was determined by X-ray analysis to show that a carbon monoxide molecule was added to the Pt−Rh bond (2.762(2) Å), resulting in an asymmetrical CO bridging structure. The similar reaction of **7a** with CO yielded another kind of CO adduct, $[Pt_2\{Rh(\mu\text{-Cl})(\mu\text{-CO})L\}(\mu\text{-dpmp})_2L](PF_6)_2$ (**11a**), which did not regenerate the starting complex **7a**. Reaction of **6a** with an electron-deficient alkyne, $HC{\equiv}CCO_2Me$, led to the alkyne-inserted compound $[Pt(\mu\text{-HC}{=}CCO_2Me)Pt\{RhClL\}(\mu\text{-dpmp})_2L](PF_6)_2$ (**12a**), in which the alkyne is site-selectively inserted into the Pt−Pt bond. The present results suggested that the Rh center has an electrophilic property and the Pt_2 unit has a nucleophilic one in the linear Pt_2Rh structure.

Introduction

Chemistry of metal−metal-bonded di-, tri-, and polynuclear complexes is closely implicated in developing industrial heterogeneous catalysts, and the construction of new transition-metal assembly is a significant subject since metal−metal-bonded small-size clusters could serve as minimal models for the surface of heterogeneous catalysts and have potential to promote new homogeneous catalytic reactions which are not established by mononuclear centers.[1] In designing such cluster cores, one of the most significant problems is how to stabilize the cluster aggregation to resist cluster fragmentation during chemical reactions. The choice of supporting ligands such as multidentate phosphines is thus important to develop new metal assemblages.[1b,2−4] With this respect, the tridentate phosphine ligand, bis(diphenylphosphinomethyl)phenylphosphine (dpmp), has attracted our attention because the dpmp ligand has versatile bridging and chelating coordination behaviors for di- and trinuclear metal centers.[5−10]

* To whom correspondence should be addressed. Fax: +81 742-20-3399. E-mail: tanase@cc.nara-wu.ac.jp.
† Nara Women's University.
‡ Toho University.

(1) (a) Adams, D. A., Cotton, F. A., Eds. *Ctalysis by Di- and Polynuclear Metal Cluster Complexes*; Wiley-VCH: New York, 1998. (b) Balch, A. L. In *Homogeneous Catalysis with Metal Phosphine Complexes*; Pignolet, L. H., Ed.; Plenum Press: New York, 1983; p 167. (c) Sinfelt, J. H. *Bimetallic Catalysis: Discoveries, Concepts and Applications*; Wiley: New York, 1983. (d) Guczi, L. In *Metal Clusters in Catalysis*; Gates, B. C., Guczi, L., Knozinger, H., Eds.; Elsevier: New York, 1986. (e) Farrygia, L. J. *Adv. Organomet. Chem.* **1990**, *31*, 301. (f) Braunstein, P.; Rose, J. *Comprehensive Organometallic Chemistry II*; Adams, R. D., Ed.; Elsevier: New York, 1995; Vol. 10, p 351.

(2) Puddephatt, R. J. *Chem. Soc. Rev.* **1983**, *12*, 99.
(3) Mayer, H. A.; Kaska, W. C. *Chem. Rev.* **1994**, *94*, 1239.
(4) Puddephatt, R. J.; Manojlovic-Muir, L.; Muir, K. W. *Polyhedron* **1990**, *9*, 2767, and references therein.
(5) Balch, A. L. In *Progress in Inorganic Chemistry*; Lippard, S. J., Ed., 1994; Vol. 42, p 239, and references therein.
(6) Tanase, T.; Yamamoto, Y. *Trends Organomet. Chem.* **1999**, *3*, 31.
(7) (a) Tanase, T.; Ukaji, H.; Takahata, H.; Toda, T.; Yamamoto, Y. *Organometallics* **1998**, *17*, 196. (b) Tanase, T.; Takahata, H.; Yamamoto, Y. *Inorg. Chim. Acta* **1997**, *264*, 5. (c) Tanase, T.; Takahata, H.; Ukaji, H.; Hasegawa, M.; Yamamoto, Y. *J. Organomet. Chem.* **1997**, *538*, 247.
(8) Tanase, T.; Ukaji, H.; Igoshi, T.; Yamamoto, Y. *Inorg. Chem.* **1996**, *35*, 4114.
(9) Tanase, T.; Toda, T.; Yamamoto, Y. *Inorg. Chem.* **1997**, *36*, 1571.
(10) (a) Tanase, T.; Masuda, K.; Hamaguchi, M.; Begum, R. A.; Yano, S. *Inorg. Chim. Acta* **2000**, *299*, 99. (b) Tanase, T.; Hamaguchi, M.; Begum, R. A.; Yano, S.; Yamamoto, Y. *Chem. Commun.* **1999**, 745. (c) Tanase, T.; Igoshi, T.; Yamamoto, Y. *Inorg. Chim. Acta* **1997**, *256*, 61. (d) Tanase, T.; Takahata, H.; Hasegawa, M.; Yamamoto, Y. *J. Organomet. Chem.* **1997**, *545/546*, 531.

10.1021/om000843z CCC: $20.00
Publication on Web 02/08/2001

Scheme 1

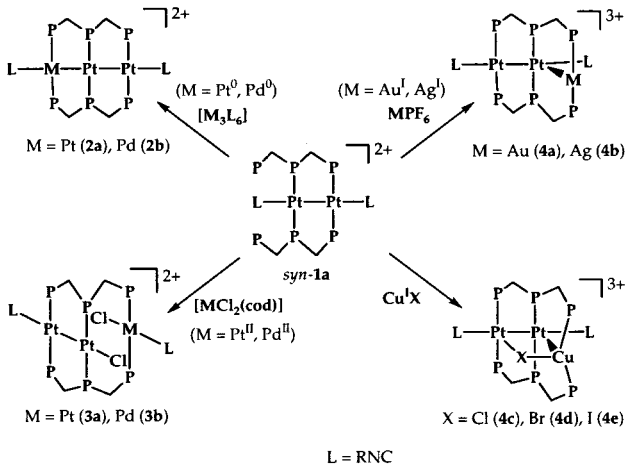

Scheme 2

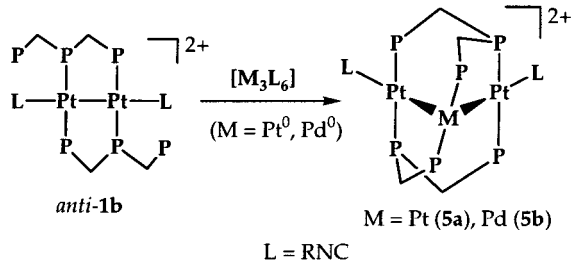

We have recently established a new strategic synthetic route to homo- and heterotrimetallic clusters with PtPtM and PtMPt metal cores by using the isomeric diplatinum complexes *syn*- and *anti*-$[Pt_2(\mu\text{-dpmp})_2(\text{isocyanide})_2]^{2+}$ (*syn*-**1a**, *anti*-**1b**) as precursors (Schemes 1 and 2).[7] The *syn*-type dimer **1a** was readily transformed by treatment with d^{10} M(isocyanide)$_2$ fragments and d^8 metal species $[MCl_2(cod)]$ to novel linear homo- and heterotrinuclear clusters, *linear*-$[Pt_2M(\mu\text{-dpmp})_2(\text{isocyanide})_2]^{2+}$ (M = Pt (**2a**), Pd (**2b**)),[7] and to dimer−monomer combined complexes, $[Pt_2MCl_2(\mu\text{-dpmp})_2(\text{isocyanide})_2]^{2+}$ (M = Pt (**3a**), Pd (**3b**)),[8] respectively (Scheme 1). The Pt_2 dimer **1a** was also reacted with d^{10} group 11 metal ions to afford $[Pt_2M(dpmp)_2(\text{isocyanide})_2](PF_6)_2$ (M = Au (**4a**), Ag (**4b**)) and $[Pt_2CuX(dpmp)_2(\text{isocyanide})_2](PF_6)_2$ (X = Cl (**4c**), Br (**4d**), I (**4e**)), which involved deformed Pt_2M cluster cores.[9] In contrast, the *anti*-type dimer **1b** reacted with a d^{10} M(isocyanide) fragment to give the A-frame trinuclear clusters *A-frame*-$[PtMPt(\mu\text{-dpmp})_2(\text{isocyanide})_2]^{2+}$ (M = Pt (**5a**), Pd (**5b**))[7] (Scheme 2). The inserted position of the additional metal interestingly depends on the diplatinum precursors used.

In the present study, we have applied this synthetic methodology to group 9 metal ions in hoping to develop new Pt_2Rh and Pt_2Ir clusters. The use of Pt/Rh and Pt/Ir mixed-metal catalysts is quite important in the scrubbing of automobile exhaust gases and in petroleum refining;[1c−f] however, metal−metal-bonded Pt/Rh and Pt/Ir trimetallic cluster complexes are still very rare. The structurally characterized examples are limited to the Ir_2Pt clusters $[PtIr_2(CO)_2(\mu\text{-CO})(\mu\text{-dppm})_3]$ and $[PtIr_2(CO)_4(\mu\text{-CO})(\mu\text{-dppm})_2]$[11] and the Rh_2Pt clusters $[Cp^*_2Rh_2Pt(\mu\text{-CO})_2(CO)(PPh_3)]$ and $[Cp^*_2Rh_2Pt(\mu\text{-H})(\mu\text{-CO})_2(CO)(PPh_3)]$,[12] all of which possessed triangular metal frameworks. Here, we wish to report successful isolation and characterization of the new linear Pt_2Rh and Pt_2Ir clusters $[Pt_2\{MCl(XylNC)\}(\mu\text{-dpmp})_2(XylNC)]^{2+}$ (M = Rh(I) (**6a**), Ir(I) (**6b**)), together with isomeric clusters with a Pt−Pt−M A-frame array, $[Pt_2\{M(\mu\text{-Cl})(XylNC)\}(\mu\text{-dpmp})_2(XylNC)]^{2+}$ (M = Rh (**7a**), Ir (**7b**)). We have also examined reactions of **6a** with small organic molecules, such as isocyanide, carbon monoxide, and an electron-deficient alkyne, to elucidate the nature of the cluster core. Preliminary results have already been reported.[13]

Experimental Section

Organic solvents were dried and freshly distilled prior to use. Other reagents were of the best commercial grade and were used as received. *syn*-$[Pt_2(dpmp)_2(XylNC)_2](PF_6)_2$ (**1a**),[7a] $[RhCl(cod)]_2$,[14] and $[IrCl(cod)]_2$[15] were prepared by the methods already reported. ^{13}C-enriched carbon monoxide, ^{13}CO (99%), was purchased from Isotec Inc. All reactions were carried out under a nitrogen atmosphere with standard Schlenk and vacuum line techniques.

Measurement. ^{1}H NMR spectra were measured on a Bruker AC250 instrument at 250 MHz and a Varian Gemini 2000 instrument at 300 MHz. Chemical shifts were calibrated to tetramethylsilane as an external reference. $^{31}P\{^1H\}$ NMR spectra were recorded by the same instruments at 101 MHz (AC250) and 121 MHz (Gemini2000), chemical shifts being calibrated to 85% H_3PO_4 as an external reference. Infrared absorption spectra were recorded with Jasco FT/IR-5300 and FT/IR-400 spectrometers. Electronic absorption spectra (UV−vis) were measured on Jasco Ubest30 and Shimadzu UV3100 spectrometers. Conductivities of **6a** and **11a** in acetone were measured at 23 °C with a Toa Denpa model WM-22EP conductivity bridge, and the reported molar conductivities (S cm^2 mol^{-1}) were derived from the slopes of a plot of conductivity (S cm^{-1}) versus concentration (mol cm^{-3}).

Preparation of $[Pt_2\{RhCl(XylNC)\}(\mu\text{-dpmp})_2(XylNC)](PF_6)_2$ (6a) and $[Pt_2\{Rh(\mu\text{-Cl})(XylNC)\}(\mu\text{-dpmp})_2(XylNC)](PF_6)_2$ (7a). To a dichloromethane solution (50 mL) containing *syn*-$[Pt_2(\mu\text{-dpmp})_2(XylNC)_2](PF_6)_2$ (**1a**) (1002 mg, 5.12 mmol) was added a dichloromethane solution (10 mL) of $[RhCl(cod)]_2$ (130 mg, 2.64 mmol) at room temperature. The solution was stirred at room temperature for 18 h. The solvent was removed under reduced pressure, and the residue was washed with benzene (5 mL × 3 times). The residue was extracted with dichloromethane, and the extract was passed through a glass filter and was concentrated to ca. 5 mL. Diethyl ether was carefully added to the solution to give reddish orange crystals of $[Pt_2\{RhCl(XylNC)\}(\mu\text{-dpmp})_2(XylNC)](PF_6)_2$ (**6a**), which were collected by removing mother liquor via cannula, washed with diethyl ether, and dried under vacuum (612 mg, yield 58%). Anal. Calcd for $C_{82}H_{76}N_2F_{12}P_8ClPt_2Rh$: C, 47.04; H, 3.66; N, 1.34. Found: C, 47.30; H, 3.65; N, 1.09. IR (Nujol): 2160, 2120 (N≡C) cm^{-1}. ^{1}H NMR (250 MHz) (acetone-d_6): δ 1.39 (s, *o*-Me), 1.48 (s, *o*-Me), 3.3−5.2 (m, CH_2), 6.5−8.4 (m, Ar). $^{31}P\{^1H\}$ NMR (101 MHz) (acetone-d_6): δ −4.66 (m, $^1J_{PtP}$ = 2466 Hz, 2P), 4.64

(11) Sterenberg, B. T.; Jenkins, H. A.; Puddephatt, R. J. *Organometallics* **1999**, *18*, 219.

(12) (a) Boag, N. M.; Green, M.; Mills, R. M.; Pain, G. N.; Stone, F. G. A.; Woodward, P. *Chem. Commun.* **1980**, 1171. (b) Green, M.; Howard, J. A. K.; Mills, R. M.; Pain, G. N.; Stone, F. G. A.; Woodward, P. *Chem. Commun.* **1981**, 869. (c) Green, M.; Mills, R. M.; Pain, G. N.; Stone, F. G. A.; Woodward, P. *J. Chem. Soc., Dalton Trans.* **1982**, 1321. (d) Green, M.; Mills, R. M.; Pain, G. N.; Stone, F. G. A.; Woodward, P. *J. Chem. Soc., Dalton Trans.* **1982**, 1309.

(13) Tanase, T.; Toda, H.; Kobayashi, K.; Yamamoto, Y. *Organometallics* **1996**, *15*, 5272.

(14) Giordano, G.; Crabtree, R. H. *Inorg. Synth.* **1979**, *19*, 218.

(15) Herde, J. L.; Lambert, J. C.; Senoff, C. V. *Inorg. Synth.* **1974**, *15*, 18.

(m, $^1J_{PtP}$ = 2800 Hz, 2P), 17.65 (d × d × m, $^1J_{RhP}$ = 108 Hz, $^2J_{PP}$ = 428 Hz, 1P), 27.79 (d × d × m, $^1J_{RhP}$ = 106 Hz, $^2J_{PP}$ = 428 Hz, 1P). UV−vis (CH_2Cl_2): λ_{max} (log ϵ) 416 (4.00), 375 (4.02) nm. The mother liquor was further concentrated, and an addition of diethyl ether afforded reddish orange crystals of [Pt_2{Rh(μ-Cl)(XylNC)}(μ-dpmp)$_2$(XylNC)](PF_6)$_2$ (**7a**) (339 mg, 32%). Anal. Calcd for $C_{82}H_{76}N_2F_{12}P_8ClPt_2Rh$: C, 47.04; H, 3.66; N, 1.34. Found: C, 46.94; H, 3.62; N, 1.29. IR (Nujol): 2176, 2091 (N≡C) cm^{-1}. ^1H NMR (250 MHz) (acetone-d_6): δ 1.67 (s, *o*-Me), 1.84 (s, *o*-Me), 3.6−5.6 (m, CH_2), 6.9−8.4 (m, Ar). $^{31}P\{^1H\}$ NMR (101 MHz) (acetone-d_6): δ −0.25 (m, $^1J_{PtP}$ = 2466 Hz, 2P), 1.64 (m, $^1J_{PtP}$ = 2810 Hz, 2P), 19.80 (d × m, $^1J_{RhP}$ = 122 Hz, 2P). UV−vis (CH_2Cl_2): λ_{max} (log ϵ) 463 (3.72) nm.

Preparation of [Pt_2{IrCl(XylNC)}(μ-dpmp)$_2$(XylNC)](PF_6)$_2$ (6b) and [Pt_2{Ir(μ-Cl)(XylNC)}(μ-dpmp)$_2$(XylNC)](PF_6)$_2$ (7b). By a procedure simliar to that mentioned above, using [IrCl(cod)]$_2$ instead of [RhCl(cod)]$_2$, reddish orange crystals of [Pt_2{IrCl(XylNC)}(μ-dpmp)$_2$(XylNC)](PF_6)$_2$·0.5CH_2Cl_2 (**6b**·0.5CH_2Cl_2) and [Pt_2{Ir(μ-Cl)(XylNC)}(μ-dpmp)$_2$(XylNC)](PF_6)$_2$·0.5CH_2Cl_2 (**7b**·0.5CH_2Cl_2) were obtained in 36% and 33% yields, respectively. For **6b**·0.5CH_2Cl_2: Anal. Calcd for $C_{82.5}H_{77}N_2F_{12}P_8Cl_2Pt_2Ir$: C, 44.52; H, 3.49; N, 1.26. Found: C, 44.18; H, 3.63; N, 1.37. IR (Nujol): 2164, 2099 (N≡C) cm^{-1}. ^1H NMR (250 MHz) (acetone-d_6): δ 1.36 (s, *o*-Me), 1.50 (s, *o*-Me), 3.3−5.2 (m, CH_2), 6.5−8.4 (m, Ar). $^{31}P\{^1H\}$ NMR (101 MHz) (acetone-d_6): δ −4.46 (m, $^1J_{PtP}$ = 2475 Hz, 2P), 0.18 (m, $^1J_{PtP}$ = 2774 Hz, 2P), 15.10 (d x m, $^2J_{PP}$ = 393 Hz, 1P), 25.88 (d × m, $^2J_{PP}$ = 393 Hz, 1P). UV−vis (CH_2Cl_2): λ_{max} (log ϵ) 461 (3.44), 373 (4.09) nm. For **7b**·0.5CH_2Cl_2: Anal. Calcd for $C_{82.5}H_{77}N_2F_{12}P_8Cl_2Pt_2Ir$: C, 44.52; H, 3.49; N, 1.26. Found: C, 44.65 H, 3.31; N, 1.21. IR (Nujol): 2160, 2056 (N≡C) cm^{-1}. ^1H NMR (250 MHz) (acetone-d_6): δ 1.00 (s, *o*-Me), 1.65 (s, *o*-Me), 3.4−5.5 (m, CH_2), 6.6−8.3 (m, Ar). $^{31}P\{^1H\}$ NMR (101 MHz) (acetone-d_6): δ 1.26 (m, $^1J_{PtP}$ = 2466 Hz, 2P), 6.33 (m, $^1J_{PtP}$ = 2837 Hz, 2P), 19.20 (m, 2P). UV−vis (CH_2Cl_2): λ_{max} 566 (3.95), 395 (4.47), 317 (4.70) nm.

Preparation of [Pt_2{RhCl(XylNC)$_2$}(μ-dpmp)$_2$(XylNC)](PF_6)$_2$ (8a). To a dichloromethane solution (5 mL) containing [Pt_2{RhCl(XylNC)}(μ-dpmp)$_2$(XylNC)](PF_6)$_2$ (**6a**) (66 mg, 0.031 mmol) was added 8.3 mg of XylNC (0.063 mmol) at room temperature. The reaction solution was stirred at room temperature for 3 h. The solvent was removed under reduced pressure, and the residue was washed with diethyl ether. The residue was extracted with dichloromethane, and the extract was passed through a glass filter and was concentrated to ca. 2 mL. Diethyl ether was carefully added to the solution to give yellow crystals of [Pt_2{RhCl(XylNC)$_2$}(μ-dpmp)$_2$(XylNC)](PF_6)$_2$ (**8a**), which were collected, washed with diethyl ether, and dried in vacuo (44 mg, yield 62%). Anal. Calcd for $C_{91}H_{85}N_3F_{12}P_8ClPt_2Rh$: C, 49.12; H, 3.85; N, 1.89. Found: C, 48.97; H, 3.68; N, 1.96. IR (Nujol): 2182, 2122 (N≡C), 836 (PF_6) cm^{-1}. ^1H NMR (300 MHz) (acetone-d_6): δ 1.44 (s, *o*-Me, 6H), 1.63 (s, *o*-Me, 12H), 3.72, 4.27, 5.56, 6.05 (m, CH_2), 6.6−8.4 (m, Ar). $^{31}P\{^1H\}$ NMR (121 MHz) (acetone-d_6): δ −6.6 (m, $^1J_{PtP}$ = 2730 Hz, 2P), −6.3 (m, $^1J_{PtP}$ = 2719 Hz, 2P), 14.5 (d × m, $^1J_{RhP}$ = 84 Hz, 2P). UV−vis (CH_2Cl_2): λ_{max} (log ϵ) 427 (4.88), 372 (4.88), 335 (4.84) nm.

Preparation of [Pt_2{Rh(XylNC)$_3$}(μ-dpmp)$_2$(XylNC)](PF_6)$_3$ (9a) and [Pt_2{Ir(MesNC)$_3$}(μ-dpmp)$_2$(MesNC)](PF_6)$_3$ (9b). To a dichloromethane solution (5 mL) containing **6a** (95 mg, 0.045 mmol) was added 94 mg of XylNC (0.72 mmol) at room temperature, and the reaction solution was stirred for 3 h. The solvent was removed under reduced pressure, and the residue was washed with diethyl ether. The residue was crystallized from a CH_2Cl_2/Et_2O mixed solvent to afford yellow microcrystals of [Pt_2{Rh(XylNC)$_3$}(μ-dpmp)$_2$(XylNC)](PF_6)$_3$ (**9a**) (66 mg, yield 59%). Anal. Calcd for $C_{100}H_{94}N_4F_{18}P_9Pt_2Rh$: C, 48.71; H, 3.84; N, 2.27. Found: C, 48.64; H, 3.90; N, 2.03. IR (Nujol): 2156, 2121 br (N≡C), 837 (PF_6) cm^{-1}. ^1H NMR (300 MHz) (CD_2Cl_2): δ 1.36 (s, *o*-Me, 6H), 1.47 (s, *o*-Me, 12H), 1.54 (s, *o*-Me, 6H), 3.3−5.7 (m, CH_2), 6.5−8.4 (m, Ar). $^{31}P\{^1H\}$ NMR (121 MHz) (acetone-d_6): δ −7.4 (m, $^1J_{PtP}$ = 2635 Hz, 2P), −6.4 (m, $^1J_{PtP}$ = 2698 Hz, 2P), 14.5 (d × m, $^1J_{RhP}$ = 104 Hz, 2P). UV−vis (CH_2Cl_2): λ_{max} (log ϵ) 418 (4.76), 370 (4.88), 333 (4.79) nm.

A reaction, similar to that mentioned above, of **6b**·0.5CH_2Cl_2 (58 mg, 0.027 mmol) with mesityl isocyanide (MesNC) (38 mg, 0.21 mmol) for 1.5 h at room temperature afforded yellow crystals of [Pt_2{Ir(MesNC)$_3$}(μ-dpmp)$_2$(MesNC)](PF_6)$_3$ (**9b**) in 72% yield (50.1 mg). Anal. Calcd for $C_{104}H_{102}N_4F_{18}P_9Pt_2Ir$: C, 47.84; H, 3.94; N, 2.15. Found: C, 48.29; H, 4.05; N, 2.19. IR (Nujol): 2159, 2127 br (N≡C), 841 (PF_6) cm^{-1}. ^1H NMR (300 MHz) (acetone-d_6): δ 1.50, 1.53, 1.94 (s, *o*-Me), 1.33, 1.38, 2.22, 2.27 (*s*, *p*-Me), 3.7−6.2 (m, CH_2), 6.6−8.5 (m, Ar). $^{31}P\{^1H\}$ NMR (121 MHz) (acetone-d_6): δ −22.6 (m, 2P), −12.3 (m, $^1J_{PtP}$ = 2793 Hz, 2P), −6.8 (m, $^1J_{PtP}$ = 2661 Hz, 2P). UV−vis (CH_2Cl_2): λ_{max} (log ϵ) 418 (4.76), 370 (4.88), 333 (4.79) nm.

Preparation of [Pt_2{RhCl(XylNC)(μ-CO)}(μ-dpmp)$_2$(XylNC)](PF_6)$_2$ (10a). Into a dichloromethane solution (5 mL) containing **6a** (63 mg, 0.030 mmol) CO gas was passed for 5 min at room temperature. By that time the color of the solution changed from orange to yellow. Diethyl ether was added to the solution, and the solution was then allowed to stand at room temperature to afford yellow crystals of [Pt_2{RhCl(XylNC)(μ-CO)}(μ-dpmp)$_2$(XylNC)](PF_6)$_2$·0.5CH_2Cl_2 (**10a**·0.5CH_2Cl_2), which were collected by removing mother liquor via cannula, washed with diethyl ether, and dried under vacuum (45 mg, yield 70%). Anal. Calcd for $C_{83.5}H_{77}N_2OF_{12}P_8Cl_2Pt_2Rh$: C, 46.34; H, 3.59; N, 1.29. Found: C, 46.53; H, 3.73; N, 1.38. IR (Nujol): 2160, 2122 (N≡C), 1839 (C═O), 841 (PF_6) cm^{-1}. ^1H NMR (300 MHz) (acetone-d_6): δ 1.52 (s, *o*-Me), 1.85 (s, *o*-Me), 4.1−6.2 (m, CH_2), 6.8−8.3 (m, Ar). $^{31}P\{^1H\}$ NMR (121 MHz) (acetone-d_6): δ −8.93 (m, $^1J_{PtP}$ = 2527 Hz, 1P), −7.14 (m, $^1J_{PtP}$ = 2581 Hz, 1P), −3.81 (m, $^1J_{PtP}$ = 2795 Hz, 1P), 1.81 (m, $^1J_{PtP}$ = 2829, 1P), 20.02 (d × d × m, $^1J_{RhP}$ = 119 Hz, $^2J_{PP}$ = 397 Hz, 1P), 31.72 (d × d × m, $^1J_{RhP}$ = 118 Hz, $^2J_{PP}$ = 397 Hz, 1P). UV−vis (CH_2Cl_2): λ_{max} (log ϵ) 354 sh (4.75), 290 (4.98) nm.

Preparation of [Pt_2{Rh(μ-Cl)(XylNC)(μ-CO)}(μ-dpmp)$_2$(XylNC)](PF_6)$_2$ (11a). CO gas was passed through a dichloromethane solution (5 mL) containing **7a** (67 mg, 0.032 mmol) for 5 min at room temperature. The color of the solution changed from orange to yellow. After an addition of diethyl ether the solution was put into a refrigerator to give yellow crystals of [Pt_2{Rh(μ-Cl)(XylNC)(μ-CO)}(μ-dpmp)$_2$(XylNC)](PF_6)$_2$ (**11a**) (47 mg, yield 70%). Anal. Calcd for $C_{83}H_{76}N_2OF_{12}P_8ClPt_2Rh$: C, 46.98; H, 3.61; N, 1.32. Found: C, 46.99; H, 3.76; N, 1.26. IR (Nujol): 2162, 2124 (N≡C), 1818 (C═O), 835 (PF_6) cm^{-1}. ^1H NMR (300 MHz) (acetone-d_6): δ 1.58 (s, *o*-Me), 1.89 (s, *o*-Me), 3.9−6.1 (m, CH_2), 6.8−8.2 (m, Ar). $^{31}P\{^1H\}$ NMR (121 MHz) (acetone-d_6): δ −3.77 (m, $^1J_{PtP}$ = 2535 Hz, 2P), −2.57 (m, $^1J_{PtP}$ = 2940 Hz, 2P), 21.75 (d × m, $^1J_{RhP}$ = 95 Hz, 2P). UV−vis (CH_2Cl_2): λ_{max} (log ϵ) 455 (4.48), 388 (4.39), 328 (4.47), 294 (4.73) nm.

Preparation of [Pt_2{RhCl(XylNC)}(μ-HC═CCO$_2$Me)(μ-dpmp)$_2$(XylNC)](PF_6)$_2$ (12a). To a dichloromethane solution (5 mL) containing **6a** (49 mg, 0.023 mmol) was added propiolic acid methyl ester (81 mg, 0.96 mmol) at room temperature. The solution was stirred at room temperature for 12 h and then heated at reflux for 8 h, by which the color became deep red. The solvent was removed under reduced pressure, and the residue was washed with diethyl ether. The residue was crystallized from a CH_2Cl_2/Et_2O mixed solvent to give red microcrystals of [Pt_2{RhCl(XylNC)}(μ-dpmp)$_2$(μ-HC═CCO$_2$Me)(XylNC)](PF_6)$_2$ (**12a**) (19.0 mg, yield 38%). Anal. Calcd for $C_{86}H_{80}N_2O_2F_{12}P_8ClPt_2Rh$: C, 47.43; H, 3.70; N, 1.29. Found: C, 47.05; H, 3.71; N, 1.22. IR (Nujol): 2147 sh, 2130 (N≡C), 1688 (C═O), 1557 (C═C), 838 (PF_6) cm^{-1}. ^1H NMR (300 MHz) (CD_2Cl_2): δ 1.37 (s, *o*-Me), 1.72 (s, *o*-Me), 3.37 (s, CO_2CH_3), 3.2−5.8 (m, CH_2), 5.12 (br s, C═CH), 6.4−8.2 (m, Ar). $^{31}P\{^1H\}$ NMR (121 MHz) (CD_2Cl_2): δ 26.4 (d × d × m, $^1J_{RhP}$ = 88 Hz, $^2J_{PP}$ = 438 Hz, 1P), 5.9 (d × d × m, $^1J_{RhP}$ = 89 Hz, $^2J_{PP}$ = 438

Table 1. Crystallographic and Experimental Data for $[Pt_2\{RhCl(XylNC)\}(\mu\text{-dpmp})_2(XylNC)](PF_6)_2$ (6a), $[Pt_2\{IrCl(XylNC)\}(\mu\text{-dpmp})_2(XylNC)](PF_6)_2$ (6b), and $[Pt_2\{Rh(\mu\text{-Cl})(XylNC)\}(\mu\text{-dpmp})_2(XylNC)](PF_6)_2$ (7a)

	6a·$2CH_2Cl_2$	**6b**	**7a**·$4CH_2Cl_2$
formula	$C_{84}H_{80}N_2P_8F_{12}Cl_5Pt_2Rh$	$C_{82}H_{76}N_2P_8F_{12}ClPt_2Ir$	$C_{86}H_{84}N_2P_8F_{12}Cl_9Pt_2Rh$
fw	2263.69	2183.14	2433.56
cryst syst	monoclinic	triclinic	monoclinic
space group	$P2_1/c$ (No. 14)	$P\bar{1}$ (No. 2)	Pn (No. 7)
a, Å	24.951(2)	15.987(6)	14.892(7)
b, Å	15.772(1)	22.041(6)	20.813(6)
c, Å	25.526(4)	15.145(7)	16.742(3)
α, deg		103.31(3)	
β, deg	119.20(1)	95.86(4)	113.50(2)
γ, deg		74.68(2)	
V, Å^3	8769	5004	4758
Z	4	2	2
T, °C	−80	23	−95
D_{calcd}, g cm^{-3}	1.714	1.449	1.698
abs coeff, cm^{-1}	37.65	43.50	35.46
trans factor	0.79−1.00	0.54−1.00	0.71−1.00
machine	CAD4	AFC5S	AFC5S
scan method	$\omega-2\theta$	$\omega-2\theta$	$\omega-2\theta$
scan speed, min^{-1}	2−16 variable	8	8
2θ range, deg	$3 < 2\theta < 45$	$3 < 2\theta < 45$	$3 < 2\theta < 50$
h,k,l range	$+h, +k, \pm l$	$+h, \pm k, \pm l$	$+h, +k, \pm l$
no. of unique data	11 938	13 171	8640
no. of obsd data ($I > 3\sigma(I)$)	10 013	6574	6509
no. of variables	1028	553	680
data/param	9.74	11.89	9.57
R^a	0.027	0.062	0.049
$R_w{}^a$	0.040	0.069	0.052
GOF^b	1.71	2.34	1.72

^{a} $R = \sum||F_o| - |F_c||/\sum|F_o|$; $R_w = [\sum w(|F_o| - |F_c|)^2/\sum w|F_o|^2]^{1/2}$ ($w = 1/\sigma^2(F_o)$). ^{b} GOF $= [\sum w(|F_o| - |F_c|)^2/(N_o - N_p)]^{1/2}$ (N_o = no. data, N_p = no. variables).

Table 2. Crystallographic and Experimental Data for $[Pt_2\{RhCl(XylNC)_2\}(\mu\text{-dpmp})_2(XylNC)](PF_6)_2$ (8a), $[Pt_2\{Ir(MesNC)_3\}(\mu\text{-dpmp})_2(MesNC)](PF_6)_3$ (9b), and $[Pt_2\{RhCl(\mu\text{-CO})(XylNC)\}(\mu\text{-dpmp})_2(XylNC)](PF_6)_2$ (10a)

	8a·$4CH_2Cl_2$	**9b**·$2CH_2Cl_2$	**10a**·$2.5CH_2Cl_2$
formula	$C_{95}H_{93}N_3P_8F_{12}Cl_9Pt_2Rh$	$C_{106}H_{106}N_4P_9F_{18}Cl_4Pt_2Ir$	$C_{85.5}H_{81}N_2OP_8F_{12}Cl_6Pt_2Rh$
fw	2564.73	2780.98	2334.17
cryst syst	triclinic	monoclinic	orthorhombic
space group	$P\bar{1}$ (No. 2)	$P2_1/n$ (No. 14)	$Pbca$ (No. 61)
a, Å	15.633(4)	20.111(5)	39.94(1)
b, Å	24.722(8)	22.153(4)	23.964(7)
c, Å	14.569(7)	25.835(5)	19.534(4)
α, deg	101.46(4)		
β, deg	109.77(3)	99.27(2)	
γ, deg	89.15(3)		
V, Å^3	5184	11 359	18 696
Z	2	4	8
T, °C	−137	−117	−118
D_{calcd}, g cm^{-3}	1.634	1.626	1.658
abs coeff, cm^{-1}	32.59	39.16	35.24
trans factor	0.86−1.00	0.79−1.00	0.80−1.00
machine	AFC7R	AFC7R	AFC7R
scan method	$\omega-2\theta$	$\omega-2\theta$	$\omega-2\theta$
scan speed, min^{-1}	8	8	8
2θ range, deg	$4 < 2\theta < 45$	$4 < 2\theta < 45$	$4 < 2\theta < 45$
h,k,l range	$+h, \pm k, \pm l$	$+h, +k, \pm l$	$+h, +k, +l$
no. of unique data	9762	14 705	12 124
no. of obsd data	6169 ($I > 3\sigma(I)$)	9849 ($I > 2\sigma(I)$)	6338 ($I > 2\sigma(I)$)
no. of variables	704	863	633
data/param	8.76	11.41	10.01
R^a	0.069	0.050	0.082
$R_w{}^a$	0.079	0.057	0.086
GOF^b	3.09	1.61	1.98

^{a} $R = \sum||F_o| - |F_c||/\sum|F_o|$; $R_w = [\sum w(|F_o| - |F_c|)^2/\sum w|F_o|^2]^{1/2}$ ($w = 1/\sigma^2(F_o)$). ^{b} GOF $= [\sum w(|F_o| - |F_c|)^2/(N_o - N_p)]^{1/2}$ (N_o = no. data, N_p = no. variables).

Hz, 1P), complicated peaks were observed around 2 to −15 ppm for 4P. UV−vis (CH_2Cl_2): λ_{max} (log ϵ) 471 (4.13), 341 (4.80), 307 (4.90) nm.

X-ray Crystallography. The crystals of **6a**·$2CH_2Cl_2$, **7a**·$4CH_2Cl_2$, **8a**·$4CH_2Cl_2$, **9b**·$2CH_2Cl_2$, and **10a**·$2.5CH_2Cl_2$ used in data collection were coated with Paraton N oil at low temperature, and the crystal of **6b** was sealed into a glass tube capillary (0.7 mm o.d.) with a droplet of mother liquor. Crystal data and experimental conditions are summarized in Tables 1 and 2. The data of **6a**·$2CH_2Cl_2$ were collected on a Enraf-Nonius CAD4 diffractometer equipped with graphite-monochromated Mo Kα (λ = 0.71069 Å) radiation at −80 °C, and those of **6b** and **7a**·$4CH_2Cl_2$ were collected on a Rigaku AFC5S diffractometer with Mo Kα (λ = 0.71069 Å) radiation at 23

and −95 °C, respectively. Those of **8a**·4CH_2Cl_2, **9b**·2CH_2Cl_2, and **10a**·2.5CH_2Cl_2 were collected on a Rigaku AFC7R diffractometer with Mo Kα (λ = 0.71069 Å) rotating anode radiation at −117 to −137 °C. The cell constants were obtained from least-squares refinement of 20−25 reflections with 20° < 2θ < 30°. Three standard reflections were monitored every 150 reflections and showed no systematic decrease in intensity. Reflection data were corrected for Lorentz−polarization and absorption effects (ψ-scan method).

Structure Solution and Refinement. The structure of **6a**·2CH_2Cl_2 was solved by direct methods with MITHRIL.[16] The two Pt and one Rh atoms were located initially, and subsequent cycles of least-squares refinements and Fourier syntheses gave the positions of other non-hydrogen atoms. The coordinates of all hydrogen atoms were calculated at ideal positions with a C−H distance of 0.95 Å and were not refined. The structure was refined with full-matrix least-squares techniques on F minimizing $\sum w(|F_o| - |F_c|)^2$. Final refinement was carried out with anisotropic thermal parameters for all non-hydrogen atoms and converged at R = 0.027 and R_w = 0.040 ($w = 1/\sigma^2(F_o)$).

The structure of **6b** was solved and refined by procedures similar to those described for **6a**. Final full-matrix least-squares refinement was carried out with anisotropic thermal parameters for the Pt, Ir, Cl, P, and F atoms and with isotropic ones for other non-hydrogen atoms and converged at R = 0.062 and R_w = 0.069. All H atoms were calculated at idealized position and were not refined.

The structure of **7a**·4CH_2Cl_2 was solved by direct methods with SIR92.[17] The most non-hydrogen atoms were located initially, and subsequent Fourier syntheses gave the positions of other non-hydrogen atoms. The coordinates of all hydrogen atoms were calculated at ideal positions with a C−H distance of 0.95 Å and were not refined. Final refinement was carried out with anisotropic thermal parameters for the Pt, Rh, Cl, P, F, N, and C(1)−C(6) atoms and with isotropic ones for other non-hydrogen atoms and converged at R = 0.049 and R_w = 0.052.

For compound **8a**·4CH_2Cl_2, the structure was solved by Patterson methods with DIRDIF92.[18] All H atoms except those of solvents were calculated and were not refined. Final refinement was carried out with anisotropic thermal parameters for the Pt, Rh, Cl, P, and F atoms and with isotropic ones for other non-hydrogen atoms to converge at R = 0.069 and R_w = 0.079. One CH_2Cl_2 molecule was disordered and refined with four Cl and two C atoms with 0.5 occupancy each.

For compound **9b**·2CH_2Cl_2, the structure was solved by direct methods with SIR92. All H atoms except those of solvents and the disordered isocyanide were calculated and were not refined. Final refinement was carried out with anisotropic thermal parameters for the Pt, Ir, Cl, P, F, N, and C(1)−C(8) atoms and with isotropic ones for other non-hydrogen atoms to converge at R = 0.050 and R_w = 0.057. The mesityl ring C(41)−C(54) of the isocyanide bound to Ir was disordered and refined with a two-site tilting model. One CH_2Cl_2 molecule was considerably disordered and refined with two Cl (0.5 occupancy), two Cl (0.25 occupancy), one C (0.5 occupancy), and two C (0.25 occupancy).

For compound **10a**·2.5CH_2Cl_2, the structure was solved by direct methods with SIR92. All H atoms except those of solvents were calculated and were not refined. Final refinement was carried out with anisotropic thermal parameters for the Pt, Rh, Cl, P, and F atoms and with isotropic ones for other non-hydrogen atoms to converge at R = 0.082 and R_w = 0.086. One phenyl group of dpmp (C(321)−C(326)) was refined as a rigid group. The solvent molecules were significantly disordered and were refined as 2.5CH_2Cl_2.

Scheme 3

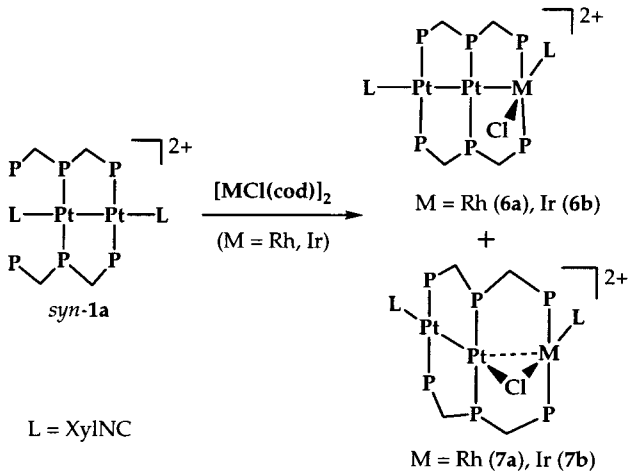

Atomic scattering factors and values of f' and f'' for Pt, Ir, Rh, Cl, P, F, N, and C were taken from the literature.[19,20] All calculations were carried out on a Digital VAX Station 3100 and Silicon Graphics Indy and O2 stations with the TEXSAN Program Package.[21] The perspective views were drawn by using the program ORTEP-II.[22] Compilation of final atomic parameters for all non-hydrogen atoms is supplied as Supporting Information.

Results and Discussion

Preparation of [Pt_2{MCl(XylNC)}(μ-dpmp)$_2$-(XylNC)](PF$_6$)$_2$ (M = Rh (6a), Ir (6b)) and [Pt_2{M(μ-Cl)(XylNC)}(μ-dpmp)$_2$(XylNC)](PF$_6$)$_2$ (M = Rh (7a), Ir (7b)). The diplatinum complex *syn*-[Pt_2(μ-dpmp)$_2$-(XylNC)$_2$](PF$_6$)$_2$ (**1a**) was treated with [RhCl(cod)]$_2$ (0.5 equiv) to afford two reddish orange complexes formulated as [Pt_2RhCl(dpmp)$_2$(XylNC)$_2$](PF$_6$)$_2$ (**6a** and **7a**) (Scheme 3). Compounds **6a** and **7a** were not interconverted to each other at room temperature and were isolated by recrystallization in 58% and 32% yields, respectively. Even upon warming at 100 °C for several hours, complexes **6a** and **7a** were not equilibrated. The IR and ^{1}H NMR spectra of both **6a** and **7a** indicated the presence of two inequivalent terminal isocyanide ligands, presumably one coordinating to a Pt atom and the other to a Rh center on the basis of their N−C stretching energies (2160, 2120 cm^{-1} for **6a** and 2176, 2091 cm^{-1} for **7a**). The electronic absorption spectra of **6a** and **7a** are quite different; that of **6a** showed a characteristic band centered at 416 nm and that of **7a** at 463 nm, suggesting a difference of the cluster frameworks between **6a** and **7a**. The ^{31}P{^{1}H} NMR spectrum of **6a** exhibited two multiplets for phosphorus atoms bound to platinum atoms at δ −4.66 (2P, $^1J_{PtP}$ = 2466) and δ 4.64 ($^1J_{PtP}$ = 2800 Hz, 2P) and two doublets of doublets of multiplets due to phosphorus atoms coordinated to the rhodium center at δ 17.65 (1P, $^1J_{RhP}$ = 108 Hz and $^2J_{PP'}$ = 428 Hz) and δ 27.79 (1P, $^1J_{RhP}$ = 106 Hz and $^2J_{PP'}$ = 428 Hz). The two phosphorus atoms

(16) Gilmore, G. J. *J. Appl. Crystallogr.* **1984**, *17*, 42.
(17) Burla, M. C.; Camalli, M.; Cascarano, G.; Giacovazzo, C.; Polidori, G.; Spagna, R.; Viterbo, D. *J. Appl. Crystallogr.* **1989**, *22*, 389.
(18) Parthasarathi, V.; Beurskens, P. T.; Slot, H. J. B. *Acta Crystallogr.* **1983**, *A39*, 860.
(19) Cromer, D. T.; Waber, J. T. *International Tables for X-ray Crystallography*; Kynoch Press: Birmingham, England, 1974; Vol. IV.
(20) Cromer, D. T. *Acta Crystallogr.* **1965**, *18*, 17.
(21) *TEXSAN Structure Analysis Package*; Molecular Structure Corp.: The Woodlands, TX, 1992.
(22) Johnson, C. K. *ORTEP-II*; Oak Ridge National Laboratory, Oak Ridge, TN, 1976.

bound to the Rh center are inequivalent and show a large *trans* coupling. The $^{31}P\{^1H\}$ NMR spectrum of **7a** consisted of two multiplets at δ −0.25 and 1.64 with ^{195}Pt satelite peaks ($^1J_{PtP}$ = 2466 and 2810 Hz) and a doublet of multiplets at δ 19.80 ($^1J_{RhP}$ = 122 Hz) in a 1:1:1 ratio.

The similar reaction of **1a** with $[IrCl(cod)]_2$ gave the analogous clusters **6b** and **7b** formulated as $[Pt_2IrCl(\mu\text{-dpmp})_2(XylNC)_2](PF_6)_2$ in 36% and 33% yields, respectively (Scheme 3). The spectroscopic features of **6b** and **7b** are similar to those of the corresponding Pt_2Rh clusters. The IR and ^1H NMR spectra showed that two different isocyanide molecules were terminally coordinated to the Pt_2Ir core. The N≡C stretching bands were observed at 2164 and 2099 cm^{-1} for **6b** and at 2160 and 2056 cm^{-1} for **7b**; the lower frequency bands appreciably shifted to the low-energy side (~30 cm^{-1}) in comparison with the corresponding Pt_2Rh complexes **6a** and **7a**. In the UV−vis spectra, an intense absorption band was observed at 463 nm for **6b** and 569 nm for **7b**. The $^{31}P\{^1H\}$ NMR spectrum of **6b** showed two multiplets at δ −4.46 and 0.18 ($^1J_{PtP}$ = 2475−2774 Hz) and two doublets of multiplets at δ 15.10 and 25.88 ($^2J_{PP'}$ = 393 Hz) in a 2:2:1:1 ratio, the latter two being assignable to two inequivalent P nuclei bound to the Ir atom. The $^{31}P\{^1H\}$ NMR spectrum of **7b** was simple and exhibited three multiplets at δ 1.26, 6.33, and 19.20 in an intensity ratio of 1:1:1; the former two were accompanied by ^{195}Pt satellites with $^1J_{PtP}$ = 2466 and 2837 Hz.

These spectral features were consistent with the asymmetrical Pt_2M (M = Rh, Ir) structures and suggested that the additional group 9 metal ion was incorporated into a terminal position of the trimetallic aggregations. Complexes **6** and **7** are unstable in air but are relatively stable as solids.

Structures of T-Shaped Pt_2M Complexes (M = Rh (6a), Ir (6b)). The detailed structures of **6a** and **6b** were determined by X-ray crystallography. ORTEP diagrams for the complex cation of **6a** are illustrated in Figure 1a,b, and selected bond distances and angles are summarized in Tables 3 and 4. The complex cation of **6a** consists of a linear Pt_2Rh core bridged by two dpmp ligands (Pt(1)−Pt(2)−Rh(1) = 177.13(1)°) (Figure 1). The terminal platinum is three-coordinate with two terminal P atoms of dpmp and an isocyanide molecule, and the central platinum is two-coordinate with two central P atoms of dpmp. The additional Rh ion sits in a terminal position of the trinuclear array and is four-coordinate with the other two terminal P atoms of dpmp, an isocyanide, and a chloride anion. The three metal units are joined by metal−metal bonds to form a 3:2:4 type structure as depicted in Chart 1. The Pt−Pt vector is almost perpendicular to the square plane of the Rh(I) ion. In other words, the $Pt(I)_2$ dinuclear core is terminally capped by the Rh(I) square planar fragment, resulting in a T-shaped LPtPtRhClL (L = XylNC) structure supported by the two dpmp ligands. This is the first example of T-shaped trimetallic clusters, whereas the T-shaped PtRh dinuclear complex with a 3:4 type structure (Chart 1), $[PtRhCl(CO)(PPh_3)(\mu\text{-bzta})_2]$ (bzta = benzothiazole-2-thiolate),[23] has been reported. The Pt(1)−Pt(2) distance indicates the presence of a Pt(I)−Pt(I) single bond as observed in the 3:3 type diplatinum complexes.[24] The Pt(2)−Rh(1) distance is slightly longer than the Pt(II)−Rh(I) distances found in the 3:5 type dinuclear complexes of $[PtRh(\mu\text{-dppm})_2(CH_3NC)_4]^{3+}$ (2.708(2) Å), $[PtRh(\mu\text{-dppm})_2(CH_3NC)_3X]^{2+}$ (X = Cl, 2.688(2) Å; X = I, 2.703(2) Å) (dppm = bis(diphenylphosphino)methane),[25] and (*trans*,*trans*)-$[PtRhCl_3(CO)(\mu\text{-}Ph_2AsCH_2PPh_2)_2]$ (2.692((1) Å),[26] but significantly shorter than that of the 4:4 type complex,

Table 3. Selected Bond Distances (Å) and Angles (deg) for $[Pt_2\{RhCl(XylNC)\}(\mu\text{-dpmp})_2(XylNC)](PF_6)_2$ (6a)[a]

Bond Distances			
Pt(1)−Pt(2)	2.6588(3)	Pt(1)−P(1)	2.309(1)
Pt(1)−P(4)	2.322(1)	Pt(1)−C(1)	1.947(6)
Pt(2)−Rh(1)	2.7537(5)	Pt(2)−P(2)	2.262(1)
Pt(2)−P(5)	2.269(1)	Rh(1)−Cl(1)	2.358(1)
Rh(1)−P(3)	2.334(1)	Rh(1)−P(6)	2.293(1)
Rh(1)−C(2)	1.884(6)	N(1)−C(1)	1.171(7)
N(1)−C(11)	1.406(7)	N(2)−C(2)	1.158(7)
N(2)−C(21)	1.431(8)		

Bond Angles			
Pt(2)−Pt(1)−P(1)	90.32(3)	Pt(2)−Pt(1)−P(4)	91.04(3)
Pt(2)−Pt(1)−C(1)	178.1(2)	P(1)−Pt(1)−P(4)	178.43(5)
P(1)−Pt(1)−C(1)	89.6(2)	P(4)−Pt(1)−C(1)	89.1(2)
Pt(1)−Pt(2)−Rh(1)	177.13(1)	Pt(1)−Pt(2)−P(2)	88.61(4)
Pt(1)−Pt(2)−P(5)	88.14(4)	Rh(1)−Pt(2)−P(2)	88.61(4)
Rh(1)−Pt(2)−P(5)	94.64(4)	P(2)−Pt(2)−P(5)	176.74(5)
Pt(2)−Rh(1)−Cl(1)	105.72(4)	Pt(2)−Rh(1)−P(3)	94.57(4)
Pt(2)−Rh(1)−P(6)	83.84(4)	Pt(2)−Rh(1)−C(2)	77.8(2)
Cl(1)−Rh(1)−P(3)	86.75(5)	Cl(1)−Rh(1)−P(6)	89.69(5)
Cl(1)−Rh(1)−C(2)	176.5(2)	P(3)−Rh(1)−P(6)	175.56(5)
P(3)−Rh(1)−C(2)	92.5(2)	P(6)−Rh(1)−C(2)	91.2(2)
C(1)−N(1)−C(11)	173.7(6)	C(2)−N(2)−C(21)	173.1(6)
Pt(1)−C(1)−N(1)	178.1(5)	Rh(1)−C(2)−N(2)	179.4(5)

[a] Estimated standard deviations are given in parentheses.

Table 4. Selected Bond Distances (Å) and Angles (deg) for $[Pt_2\{IrCl(XylNC)\}(\mu\text{-dpmp})_2(XylNC)](PF_6)_2$ (6b)[a]

Bond Distances			
Pt(1)−Pt(2)	2.652(2)	Pt(1)−P(1)	2.318(7)
Pt(1)−P(4)	2.314(7)	Pt(1)−C(1)	2.01(2)
Pt(2)−Ir(1)	2.765(2)	Pt(2)−P(2)	2.268(7)
Pt(2)−P(5)	2.258(7)	Ir(1)−Cl(1)	2.356(6)
Ir(1)−P(3)	2.323(7)	Ir(1)−P(6)	2.313(7)
Ir(1)−C(2)	1.90(2)	N(1)−C(1)	1.12(3)
N(1)−C(11)	1.37(3)	N(2)−C(2)	1.14(2)
N(2)−C(21)	1.41(3)		

Bond Angles			
Pt(2)−Pt(1)−P(1)	89.5(2)	Pt(2)−Pt(1)−P(4)	90.9(2)
Pt(2)−Pt(1)−C(1)	179.4(6)	P(1)−Pt(1)−P(4)	179.3(2)
P(1)−Pt(1)−C(1)	90.8(7)	P(4)−Pt(1)−C(1)	88.8(7)
Pt(1)−Pt(2)−Ir(1)	177.58(7)	Pt(1)−Pt(2)−P(2)	88.7(2)
Pt(1)−Pt(2)−P(5)	87.7(2)	Ir(1)−Pt(2)−P(2)	88.9(2)
Ir(1)−Pt(2)−P(5)	94.7(2)	P(2)−Pt(2)−P(5)	175.6(2)
Pt(2)−Ir(1)−Cl(1)	106.1(2)	Pt(2)−Ir(1)−P(3)	94.4(2)
Pt(2)−Ir(1)−P(6)	82.6(2)	Pt(2)−Ir(1)−C(2)	81.1(7)
Cl(1)−Ir(1)−P(3)	84.8(2)	Cl(1)−Ir(1)−P(6)	91.3(2)
Cl(1)−Ir(1)−C(2)	172.7(7)	P(3)−Ir(1)−P(6)	174.3(2)
P(3)−Ir(1)−C(2)	93.5(8)	P(6)−Ir(1)−C(2)	90.9(8)
C(1)−N(1)−C(11)	173(3)	C(2)−N(2)−C(21)	170(2)
Pt(1)−C(1)−N(1)	173(2)	Ir(1)−C(2)−N(2)	175(2)

[a] Estimated standard deviations are given in parentheses.

(23) Ciriano, M. A.; Perez-Torrente, J. J.; Lahoz, F. J.; Ora, L. A. *Inorg. Chem.* **1992**, *31*, 969.

(24) (a) Tanase, T.; Kawahara, K.; Kobayashi K.; Yamazaki, H.; Yamamoto, Y. *Inorg. Chem.* **1993**, *32*, 3682. (b) Tanase, T.; Ukaji, H.; Kudo, K.; Ohno, M.; Kobayashi K.; YamamotoY. *Organometallics* **1994**, *13*, 1374. (c) Tanase, T.; Ukaji, H.; Yamamoto, Y. *J. Chem. Soc., Dalton Trans.* **1996**, 3059, and references therein.

(25) Balch, A. L.; Catalano, V. J. *Inorg. Chem.* **1992**, *31*, 3934.

(26) Balch, A. L.; Guimerans, R. R.; Linehan, J.; Olmstead, M. M.; Oram, D. E. *Organometallics* **1985**, *4*, 1445.

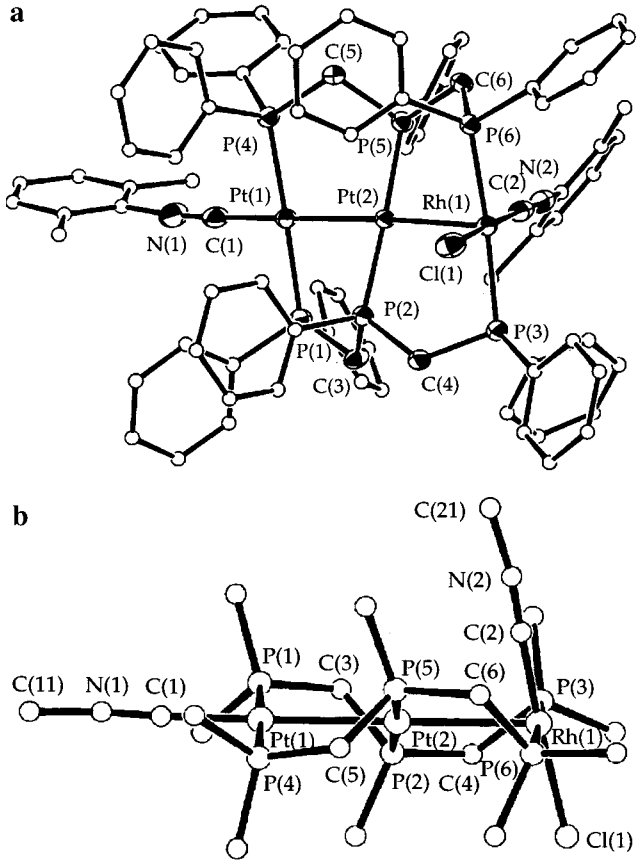

Figure 1. (a) ORTEP view of the complex cation of **6a**, $[Pt_2\{RhCl(XylNC)\}(\mu\text{-dpmp})_2(XylNC)]^{2+}$. Carbon atoms of the phenyl and xylyl groups are drawn with arbitrary circles, and hydrogen atoms are omitted for clarity. (b) ORTEP view of the complex cation of **6a**, showing the staggered P−M−P vectors. The phenyl and xylyl groups are omitted, and all atoms are drawn by ideal circles for clarity.

Chart 1

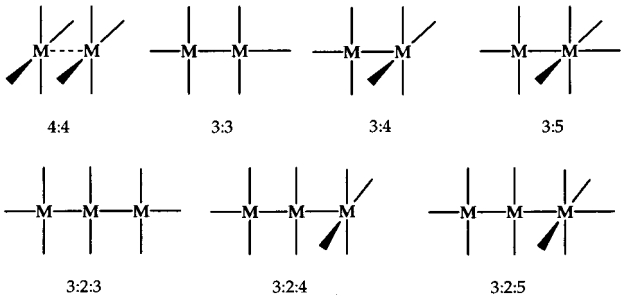

such as $[PtRh(CN)_2(^tBuNC)_2(\mu\text{-dppm})_2]^+$ (3.079(2) Å)[25] and (*trans*,*cis*)-$[RhPtCl_3(CO)(\mu\text{-}Ph_2AsCH_2PPh_2)_2]$ (3.043(1) Å),[27] in which no single bond existed between the d^8 Pt(II) and d^8 Rh(I) ions. The Pt−Rh bond can be viewed as a dative bond with the d^8 Rh(I) acting as a two-electron donor to the Pt(I) atom, and the Pt−Pt bond as a typical covalent bond with two d^9 electronic configurations. The total valence electron count for the trinuclear core is 44 with 16 apparent valence electrons for each metal.

The *trans*-PMP axes of P(1)−Pt(1)−P(4), P(2)−Pt(2)−P(5), and P(3)−Rh(1)−P(6) are mutually twisted with the torsion angles of P(1)−Pt(1)−Pt(2)−P(2) = −34.17(5)°, P(4)−Pt(1)−Pt(2)−P(5) = −35.13(5)°, P(2)−Pt(2)−Rh(1)−P(3) = 26.93(5)°, and P(5)−Pt(2)−Rh(1)−P(6) = 31.31(5)° (av 31.9°) (Figure 1b). From these twisted structures, the P(3) and P(6) atoms are chemically inequivalent, as evidenced in the ^{31}P NMR spectrum. The Cl(1) and C(2) atoms are in *trans* positions across the Rh center with Cl(1)−Rh(1)−C(2) = 176.5(1)°, and the Cl(1)−Rh(1)−C(2) axis is remarkably deformed from orthogonality with respect to the Pt−Rh axis; Pt(2)−Rh(1)−Cl(1) = 105.72(4)° and Pt(2)−Rh(1)−C(2) = 77.8(2)°. The terminal isocyanide bound to Rh(1) showed an inward bending structure, which was often observed in dinuclear Pd and Pt complexes with isocyanide ligands, such as $[Pd_2(RNC)_6](PF_6)_2$ and $[M_2(diphos)_2(RNC)_2](PF_6)_2$ (M = Pt, Pd).[24] The other isocyanide attached to the Pt(1) atom is collinear with the Pt−Pt−Rh axis, with Pt(2)−Pt(1)−C(1) = 178.1(2)° and Pt(1)−C(1)−N(1) = 178.1(5)°.

The structure of the complex **6b** (M = Ir) is isostructural with that of **6a** (M = Rh) (Table 4). The Pt_2Ir atoms are disposed in a linear array (Pt(1)−Pt(2)−Ir(1) = 177.58(7)°) and are joined by Pt−Pt and Pt−Ir bonds. The Pt(1)−Pt(2) bond length of 2.652(2) Å is comparable to that of **6b**, and the Pt(2)−Ir(1) distance of 2.765(2) Å is slightly longer by ∼0.01 Å than that of **6a**, also indicating the presence of a Pt←Ir dative bond just as observed in the 3:5 type dinuclear complex, $[PtIr(CO)Cl(\mu\text{-dpmp})_2](PF_6)_2$ (2.730(2) Å).[28] Puddephatt et al. have reported the 3:4 type PtIr complex, $[PtIr(CO)_3(\mu\text{-dppm})_2](PF_6)$,[11] where the Pt and Ir atoms are connected by a single bond (2.7674(4) Å), but the cluster framework is Y-shaped (not T-shaped) with a trigonal bipyramidal and a square planar configuration at the Ir and the Pt centers, respectively. In the triangular Ir_2Pt clusters, $[PtIr_2(CO)_2(\mu\text{-CO})(\mu\text{-dppm})_3]$ and $[PtIr_2(CO)_4(\mu\text{-CO})(\mu\text{-dppm})_2]$, the Pt−Ir bond distances are in the range 2.628(2)−2.668(2) Å.[11] As found in **6a**, the P(1)−Pt(1)−P(4), P(2)−Pt(2)−P(5), and P(3)−Ir(1)−P(6) axes are twisted with the torsion angles of P(1)−Pt(1)−Pt(2)−P(2) = 35.3(2)°, P(4)−Pt(1)−Pt(2)−P(5) = 37.2(2)°, P(2)−Pt(2)−Ir(1)−P(3) = −25.2(2)°, and P(5)−Pt(2)−Ir(1)−P(6) = −32.7(2)° (av 32.6°), and the Cl(1)−Ir(1)−C(2) axis is tilted versus the Pt(2)−Ir(1) axis with Pt(2)−Ir(1)−Cl(1) = 106.1(2)° and Pt(2)−Ir(1)−C(2) = 81.1(7)°.

Structure of Asymmetrical A-Frame Pt_2Rh Complex (7a). A perspective drawing of the complex cation of **7a** is illustrated in Figure 2, and selected bond lengths and angles are listed in Table 5. The cluster core involves two platinum and one rhodium atoms bridged by two dpmp ligands, and a chloride anion is occupied at the vertex of an asymmetrical A-frame trinuclear structure. The complex cation has a pseudo-C_s symmetry with a mirror plane comprised of the $Pt_2(\mu\text{-Cl})$-Rh unit and can be viewed as a $Pt(I)_2$ core that is terminally capped by the square planar $[Rh^ICl P_2C]$ fragment, through the Cl atom. The Pt(1)−Pt(2) distance of 2.644(1) Å is typical of a metal−metal single bond. The Pt(μ-Cl)Rh bridging structure is rather asymmetrical with Rh(1)−Cl(1) = 2.406(4) Å and Pt(2)−Cl(1) = 2.563(5) Å, the latter value indicating a weak σ-donation of the Cl(1) atom to the Pt(2) center. The Pt−Rh interatomic distance is longer by ca. 0.21 Å than that

(27) (a) Guimerans, R. R.; Wood, F. E.; Balch, A. L. *Inorg. Chem.* **1984**, *23*, 1307. (b) Balch, A. L.; Guimerans, R. R.; Linehan, J.; Wood, F. E. *Inorg. Chem.* **1985**, *24*, 2021.

(28) Balch, A. L.; Catalano, V. J. *Inorg. Chem.* **1992**, *31*, 2569.

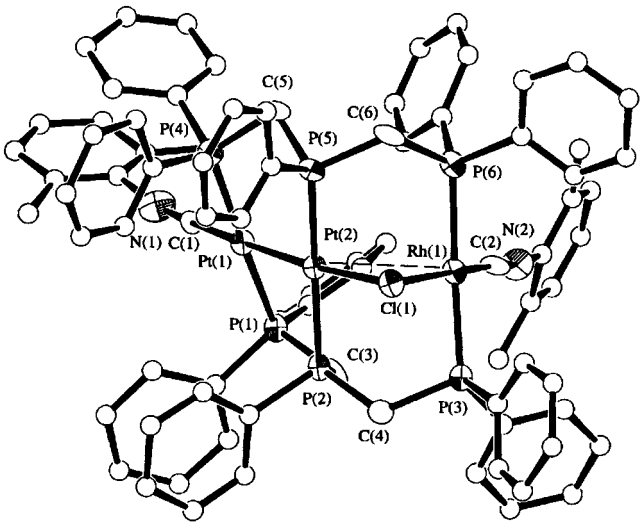

Figure 2. ORTEP plot of the complex cation of **7a**, $[Pt_2\{Rh(\mu\text{-Cl})(XylNC)\}(\mu\text{-dpmp})_2(XylNC)]^{2+}$. Carbon atoms of the phenyl and xylyl groups are drawn with arbitrary circles, and hydrogen atoms are omitted for clarity.

Table 5. Selected Bond Distances (Å) and Angles (deg) for $[Pt_2\{Rh(\mu\text{-Cl})(XylNC)\}(\mu\text{-dpmp})_2(XylNC)](PF_6)_2$ (7a)[a]

Bond Distances			
Pt(1)−Pt(2)	2.644(1)	Pt(1)−P(1)	2.289(5)
Pt(1)−P(4)	2.330(5)	Pt(1)−C(1)	1.85(1)
Pt(2)−Rh(1)	2.967(2)	Pt(2)−Cl(1)	2.563(5)
Pt(2)−P(2)	2.248(5)	Pt(2)−P(5)	2.283(5)
Rh(1)−Cl(1)	2.406(4)	Rh(1)−P(3)	2.289(5)
Rh(1)−P(6)	2.323(6)	Rh(1)−C(2)	1.86(2)
N(1)−C(1)	1.19(2)	N(1)−C(11)	1.46(3)
N(2)−C(2)	1.17(2)	N(2)−C(21)	1.46(2)
Bond Angles			
Pt(2)−Pt(1)−P(1)	92.9(1)	Pt(2)−Pt(1)−P(4)	87.9(1)
Pt(2)−Pt(1)−C(1)	177.8(6)	P(1)−Pt(1)−P(4)	177.8(2)
P(1)−Pt(1)−C(1)	89.3(6)	P(4)−Pt(1)−C(1)	89.9(6)
Pt(1)−Pt(2)−Rh(1)	125.21(4)	Pt(1)−Pt(2)−Cl(1)	174.9(1)
Pt(1)−Pt(2)−P(2)	90.1(1)	Pt(1)−Pt(2)−P(5)	96.9(1)
Rh(1)−Pt(2)−Cl(1)	50.9(1)	Rh(1)−Pt(2)−P(2)	85.0(1)
Rh(1)−Pt(2)−P(5)	94.1(1)	Cl(1)−Pt(2)−P(2)	92.7(2)
Cl(1)−Pt(2)−P(5)	80.6(2)	P(2)−Pt(2)−P(5)	172.0(2)
Pt(2)−Rh(1)−Cl(1)	55.8(1)	Pt(2)−Rh(1)−P(3)	95.8(1)
Pt(2)−Rh(1)−P(6)	86.8(1)	Pt(2)−Rh(1)−C(2)	118.5(6)
Cl(1)−Rh(1)−P(3)	83.7(2)	Cl(1)−Rh(1)−P(6)	89.9(2)
Cl(1)−Rh(1)−C(2)	173.8(6)	P(3)−Rh(1)−P(6)	170.0(2)
P(3)−Rh(1)−C(2)	94.9(6)	P(6)−Rh(1)−C(2)	92.3(5)
Pt(2)−Cl(1)−Rh(1)	73.3(1)		
C(1)−N(1)−C(11)	170(2)	C(2)−N(2)−C(21)	172(2)
Pt(1)−C(1)−N(1)	176(2)	Rh(1)−C(2)−N(2)	175(2)

[a] Estimated standard deviations are given in parentheses.

of **6a** and does not indicate the presence of a normal single bond. However, in comparison with the Cl-bridged A-frame complexes reported thus far, e.g., $[Rh_2Pd(CO)_2(\mu\text{-Cl})Cl_2(\mu\text{-dpma})_2]^+$ (Rh···Pd = 3.166(1) Å)[29] (dpma = bis(diphenylphosphinomethyl)phenylarsine), $[Pt_2Pd(\mu\text{-Cl})Cl(\mu\text{-dpmp})_2(XylNC)]^{2+}$ (Pt···Pd = 3.103(3) Å),[8] $[Rh_2(\mu\text{-Cl})(\mu\text{-dppm})_2(CO)_2]^+$ (Rh···Rh = 3.1520 Å),[30] the Pt−Rh distance of **7a** is appreciably shorter, suggesting the existence of a weak attractive interaction between the Pt and Rh atoms. A similar structure has been observed in $[Rh_3(\mu\text{-Cl})Cl(\mu\text{-dpmp})_2(\mu\text{-CO})(CO)]^+$ (Rh···Rh = 2.966(1) Å, Rh−Cl−Rh = 75.8(1)°).[31] The

Chart 2

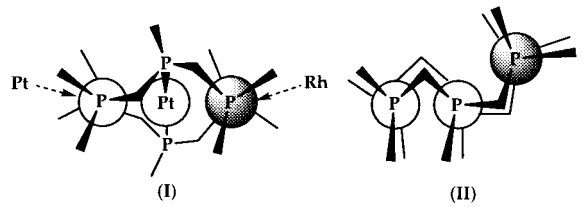

Scheme 4

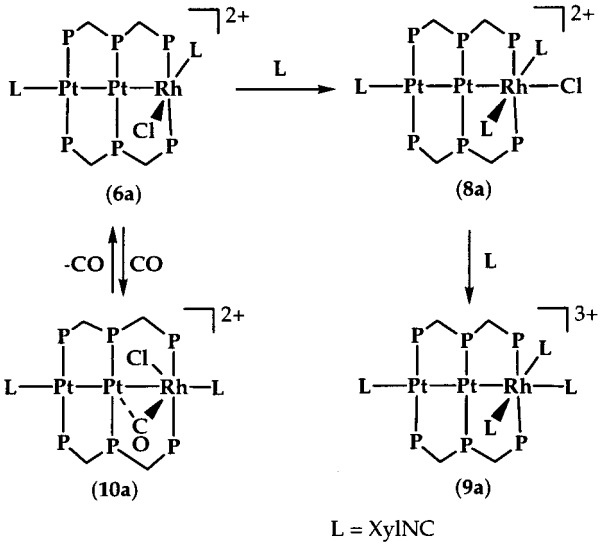

three *trans*-MP_2 axes are less twisted, compared with **6a**, with torsion angles of P(1)−Pt(1)−Pt(2)−P(2) = −21.7(2)°, P(2)−Pt(2)−Rh(1)−P(3) = −19.3(2)°, P(4)−Pt(1)−Pt(2)−P(5) = −15.7(2)°, and P(5)−Pt(2)−Rh(1)−P(6) = −17.6(2)° (av −18.6°).

On the basis of spectral similarity, complex **7b** was estimated to be isostructural with **7a**, involving an asymmetrical A-frame structure of $Pt_2(\mu\text{-Cl})Ir$ bridged by two dpmp ligands.

Arrangement of the Two dpmp Ligands. Whereas the T-shaped cluster **6a** does not have any symmetry elements, the cluster core of $Pt_2Rh(\mu\text{-dpmp})_2$ possesses a pseudo-C_2 symmetry with the axis passing through the Pt_2Rh atoms as depicted in Chart 2 (I). The C_2 symmetrical geometry (I) is relatively inflexible with respect to the linear arrangement and is retained in solution, evidenced by the ^{31}P NMR spectral pattern. As to the asymmetrical A-frame cluster **7a**, the cluster core $Pt_2Rh(\mu\text{-dpmp})_2$ has a pseudo-C_s symmetry with a mirror plane comprised of the Pt_2Rh atoms (Chart 2 (II)). The arrangement II seems to be flexible, and simultaneous rotation of two opposing methylene groups allows core structural changes in the linear structure and the more bent structure.[31] In the structure II, six P atoms were observed as an $A_2B_2C_2$ pattern in the ^{31}P NMR spectra.

Reactions of 6a with Isocyanide. Reaction of the T-shaped cluster **6a** with a regulated amount of XylNC (∼2 equiv) afforded the yellow cluster of $[Pt_2\{RhCl(XylNC)_2\}(\mu\text{-dpmp})_2(XylNC)](PF_6)_2$ (**8a**) in 62% yield (Scheme 4). The elemental analysis indicated that complex **8a** is a 1:1 adduct between **6a** and XylNC. On

(29) Bailey, D. A.; Balch, A. L.; Fossett, L. A.; Olmsted, M. M.; Reedy, P. E., Jr. *Inorg. Chem.* **1987**, *26*, 2413.
(30) Cowie, M.; Dwight, S. K. *Inorg. Chem.* **1979**, *18*, 2700.
(31) Balch, A. L.; Fossett, L. A.; Guimerans, R. R.; Olmstead, M. M. *Organometallics* **1985**, *4*, 781.

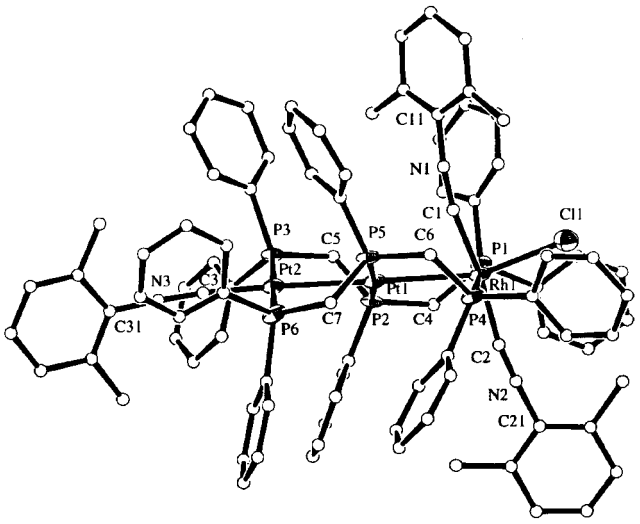

Figure 3. ORTEP diagram of the complex cation of **8a**, $[Pt_2\{RhCl(XylNC)_2\}(\mu\text{-dpmp})_2(XylNC)]^{2+}$, viewed vertical to the CPt_2RhClC_2 plane. Carbon atoms of the phenyl and xylyl groups are drawn with arbitrary circles, and hydrogen atoms are omitted for clarity.

the basis of the IR and ^1H NMR spectra, two environmentally different terminal isocyanides exist in a 2:1 ratio. In the $^{31}P\{^1H\}$ NMR spectrum of **8a**, three sets of resonances were observed at δ −6.6 ($^1J_{PtP}$ = 2730 Hz), −6.3 ($^1J_{PtP}$ = 2719 Hz), and 14.5 ($^1J_{RhP}$ = 84 Hz) in a 1:1:1 ratio, suggesting that the cluster structure in solution has C_2 or C_s symmetry. When complex **6a** was treated with excess XylNC, another yellow cluster of $[Pt_2\{Rh(XylNC)_3\}(\mu\text{-dpmp})_2(XylNC)](PF_6)_3$ (**9a**) was obtained in good yield. Complex **8a** was also converted into **9a** by treatment with XylNC. The $^{31}P\{^1H\}$ NMR spectral pattern of **9a** was almost identical to that of **8a**. The Pt_2Ir compound analogous to **9a**, $[Pt_2\{Ir(MesNC)_3\}(\mu\text{-dpmp})_2(MesNC)](PF_6)_3$ (**9b**), was prepared by the reaction of **6b** with excess MesNC.

The detailed structures of **8a** and **9b** were determined by X-ray crystallography. The ORTEP diagram for the complex cation of **8a** is shown in Figure 3, and selected bond lengths and angles are listed in Table 6. The complex cation consists of the linearly ordered Pt_2Rh atoms bridged by two dpmp ligands (Pt(2)−Pt(1)−Rh(1) = 178.02(5)°). The structure of the Pt_2 part is the same as that in **6a**, and the Rh atom adopts a distorted octahedral geometry with two isocyanides, a chloride anion, and the neighboring Pt atom, resulting in a 3:2:5 linear structure, as shown in Chart 1. The Pt(1)−Pt(2) and Pt(1)−Rh(1) bond lengths are 2.694(1) and 2.797(2) Å, respectively, both of which are slightly longer than the corresponding values in **6a**. The $[RhP_2C_2]$ equatorial plane is tilted from an orthogonal T-shaped form with Pt(1)−Rh(1)−C(1) = 71.2(5)° and Pt(1)−Rh(1)−C(2) = 102.0(6)°. The Cl atom is in a *trans* position to the Pt−Rh bond (Pt(1)−Rh(1)−Cl(1) = 161.1(1)°), and the Rh(1)−Cl(1) distance is considerably longer than is found in **6a** (2.358(1) Å). These features around the Rh center are essentially similar to the 3:5 type PtRh dinuclear complexes, $[PtRhX(\mu\text{-dppm})_2(MeNC)_3]^{2+}$ (X = Cl, I),[25] although the $\{RhXP_2(MeNC)_2\}$ fragments are less twisted versus the Pt−Rh bond in the dimers. Whereas, in the crystal structure of **8a**, the two isocyanide ligands are unequivalent, one being disposed inward to the Pt−Rh bond and the other outward from it, they are equivalent in solution on the basis of NMR spectra, presumably due to a windshield wiper-like fluxional behavior of the $\{RhClP_2(RNC)_2\}$ fragment.

Table 6. Selected Bond Distances (Å) and Angles (deg) for $[Pt_2\{RhCl(XylNC)_2\}(\mu\text{-dpmp})_2(XylNC)](PF_6)_2$ (8a)[a]

Bond Distances			
Pt(1)−Pt(2)	2.694(1)	Pt(1)−Rh(1)	2.797(2)
Pt(1)−P(2)	2.282(5)	Pt(1)−P(5)	2.277(5)
Pt(2)−P(3)	2.326(5)	Pt(2)−P(6)	2.330(6)
Pt(2)−C(3)	1.90(1)	Rh(1)−Cl(1)	2.502(6)
Rh(1)−P(1)	2.369(5)	Rh(1)−P(4)	2.328(5)
Rh(1)−C(1)	1.93(2)	Rh(1)−C(2)	2.00(2)
N(1)−C(1)	1.22(2)	N(1)−C(11)	1.41(2)
N(2)−C(2)	1.13(2)	N(2)−C(21)	1.42(2)
N(3)−C(3)	1.23(2)	N(3)−C(31)	1.39(2)
Bond Angles			
Pt(2)−Pt(1)−Rh(1)	178.02(5)	Pt(2)−Pt(1)−P(2)	87.9(1)
Pt(2)−Pt(1)−P(5)	86.7(1)	Rh(1)−Pt(1)−P(2)	90.5(1)
Rh(1)−Pt(1)−P(5)	94.9(1)	P(2)−Pt(1)−P(5)	173.7(2)
Pt(1)−Pt(2)−P(3)	89.5(1)	Pt(1)−Pt(2)−P(6)	90.4(1)
Pt(1)−Pt(2)−C(3)	176.8(4)	P(3)−Pt(2)−P(6)	177.3(2)
P(3)−Pt(2)−C(3)	93.2(4)	P(6)−Pt(2)−C(3)	86.9(4)
Pt(1)−Rh(1)−Cl(1)	161.1(1)	Pt(1)−Rh(1)−P(1)	93.1(1)
Pt(1)−Rh(1)−P(4)	82.6(1)	Pt(1)−Rh(1)−C(1)	71.2(5)
Pt(1)−Rh(1)−C(2)	102.0(6)	Cl(1)−Rh(1)−P(1)	90.3(2)
Cl(1)−Rh(1)−P(4)	96.3(2)	Cl(1)−Rh(1)−C(1)	90.0(6)
Cl(1)−Rh(1)−C(2)	96.8(6)	P(1)−Rh(1)−P(4)	171.0(2)
P(1)−Rh(1)−C(1)	93.0(5)	P(1)−Rh(1)−C(2)	85.9(6)
P(4)−Rh(1)−C(1)	93.1(5)	P(4)−Rh(1)−C(2)	87.3(6)
C(1)−Rh(1)−C(2)	173.1(8)		
C(1)−N(1)−C(11)	171(2)	C(2)−N(2)−C(21)	177(2)
C(3)−N(3)−C(31)	166(2)	Rh(1)−C(1)−N(1)	171(2)
Rh(1)−C(2)−N(2)	169(2)	Pt(2)−C(3)−N(3)	176(1)

[a] Estimated standard deviations are given in parentheses.

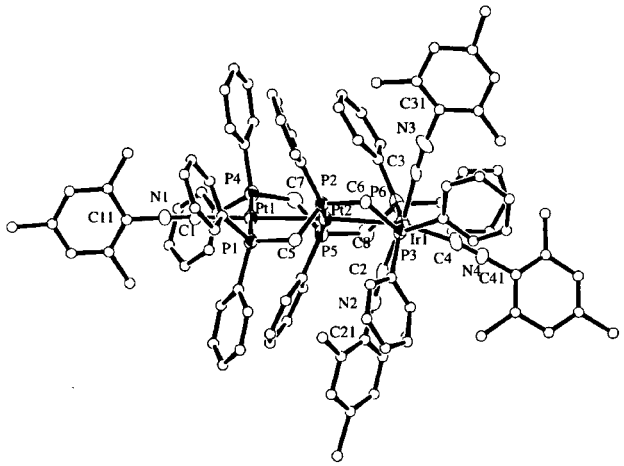

Figure 4. ORTEP diagram of the complex cation of **9b**, $[Pt_2\{Ir(MesNC)_3\}(\mu\text{-dpmp})_2(MesNC)]^{3+}$, viewed vertical to the CPt_2IrC_3 plane. Carbon atoms of the phenyl and xylyl groups are drawn with arbitrary circles, and hydrogen atoms are omitted for clarity.

The ORTEP plot for the cluster cation of **9b** is illustrated in Figure 4, and some selected bond lengths and angles are listed in Table 7. The structure is essentially similar to that of **8a**, with a linear Pt_2Ir core bridged by two dpmp ligands (Pt(1)−Pt(2)−Ir(1) = 176.48(3)°). The terminal Ir atom takes a distorted octahedral geometry with two *trans* phosphine groups, three isocyanide ligands, and the neighboring Pt atom. The similar local structure of Rh was reported in the dimer $[PtRh(\mu\text{-dppm})_2(MeNC)_4]^{3+}$.[25] The Ir−C bond

Table 7. Selected Bond Distances (Å) and Angles (deg) for $[Pt_2\{Ir(MesNC)_3\}(\mu\text{-dpmp})_2(MesNC)](PF_6)_3$ (9b)[a]

Bond Distances			
Pt(1)−Pt(2)	2.6908(8)	Pt(1)−P(1)	2.305(4)
Pt(1)−P(4)	2.305(4)	Pt(1)−C(1)	1.99(1)
Pt(2)−Ir(1)	2.8195(8)	Pt(2)−P(2)	2.247(3)
Pt(2)−P(5)	2.260(4)	Ir(1)−P(3)	2.358(3)
Ir(1)−P(6)	2.324(4)	Ir(1)−C(2)	1.98(2)
Ir(1)−C(3)	1.97(1)	Ir(1)−C(4)	2.06(1)
N(1)−C(1)	1.15(1)	N(1)−C(11)	1.39(2)
N(2)−C(2)	1.14(2)	N(2)−C(21)	1.41(2)
N(3)−C(3)	1.14(1)	N(3)−C(31)	1.44(2)
N(4)−C(4)	1.11(1)	N(4)−C(41)	1.42(2)
Bond Angles			
Pt(2)−Pt(1)−P(1)	88.94(8)	Pt(2)−Pt(1)−P(4)	90.27(8)
Pt(2)−Pt(1)−C(1)	178.7(3)	P(1)−Pt(1)−P(4)	179.0(1)
P(1)−Pt(1)−C(1)	90.1(3)	P(4)−Pt(1)−C(1)	90.7(3)
Pt(1)−Pt(2)−Ir(1)	176.48(3)	Pt(1)−Pt(2)−P(2)	87.54(8)
Pt(1)−Pt(2)−P(5)	86.18(9)	Ir(1)−Pt(2)−P(2)	91.71(8)
Ir(1)−Pt(2)−P(5)	94.52(9)	P(2)−Pt(2)−P(5)	173.7(1)
Pt(2)−Ir(1)−P(3)	90.55(8)	Pt(2)−Ir(1)−P(6)	81.70(9)
Pt(2)−Ir(1)−C(2)	71.9(4)	Pt(2)−Ir(1)−C(3)	100.6(3)
Pt(2)−Ir(1)−C(4)	163.0(3)	P(3)−Ir(1)−P(6)	167.6(1)
P(3)−Ir(1)−C(2)	93.2(4)	P(3)−Ir(1)−C(3)	83.6(3)
P(3)−Ir(1)−C(4)	94.5(4)	P(6)−Ir(1)−C(2)	93.5(4)
P(6)−Ir(1)−C(3)	88.4(4)	P(6)−Ir(1)−C(4)	95.6(4)
C(2)−Ir(1)−C(3)	171.8(5)	C(2)−Ir(1)−C(4)	91.6(5)
C(3)−Ir(1)−C(4)	96.1(5)		
C(1)−N(1)−C(11)	177(1)	C(2)−N(2)−C(21)	174(1)
C(3)−N(3)−C(31)	174(1)	C(4)−N(4)−C(41)	179(1)
Pt(1)−C(1)−N(1)	178(1)	Ir(1)−C(2)−N(2)	175(1)
Ir(1)−C(3)−N(3)	176(1)	Ir(1)−C(4)−N(4)	171(1)

[a] Estimated standard deviations are given in parentheses.

length to the apical isocyanide (Ir(1)−C(4) = 2.06(1) Å) is longer than those to the equatorial ones (Ir(1)−C(2) = 1.98(2) Å and Ir(1)−C(3) = 1.97(1) Å), due to a *trans* effect of the metal−metal bond. The tilted nature of the $\{IrP_2(XylNC)_3\}$ fragment, as observed in **8a**, $[PtRhX(\mu\text{-dppm})_2(MeNC)_3]^{2+}$, and $[PtRh(\mu\text{-dppm})_2(MeNC)_4]^{3+}$,[25] is also observed with Pt(2)−Ir(1)−C(2) = 71.9(4)°, Pt(2)−Ir(1)−C(3) = 100.6(3)°, and Pt(2)−Ir(1)−C(4) = 163.0(3)°. Both the Pt−Pt and Pt−Ir bonds are slightly elongated in comparison with **6b** (Pt(1)−Pt(2) = 2.6908(8) Å, Pt(2)−Ir(1) = 2.8195(8) Å).

The X-ray analyses of **8a** and **9b** clearly demonstrated that the added isocyanide molecules attached exclusively to the electron-deficient group 9 metal center with 16 valence electrons in **6** to form the saturated octahedral metal center with 18 valence electrons. Although the detailed mechanism was not clear in this study, the geometry around Rh of **8a** suggested the possibility that an initial attack of isocyanide occurred at the central Pt and a subsequent migration from Pt to Rh led to formation of **8a** as a thermodynamically stable compound.

Reactions of 6a and 7a with CO. Complex **6a**, treated with carbon monoxide (1 atm), was rapidly converted into the yellow cluster $[Pt_2\{RhCl(\mu\text{-CO})(XylNC)\}(\mu\text{-dpmp})_2(XylNC)](PF_6)_2$ (**10a**), which was isolated as the crystalline form under CO atmosphere in good yield (Scheme 4). Further, complex **10a** readily restored the starting complex **6a** in an almost quantitative yield by bubbling dinitrogen gas into the solution. The binding of a CO molecule to **6a** was carried out in a reversible way, which could be monitored by electronic absorption spectra. The IR spectrum of **10a** (Nujol mull) showed the NC stretching bands at 2160 and 2122 cm^{-1} and the CO stretch at 1839 cm^{-1} (the ν_{CO} band was

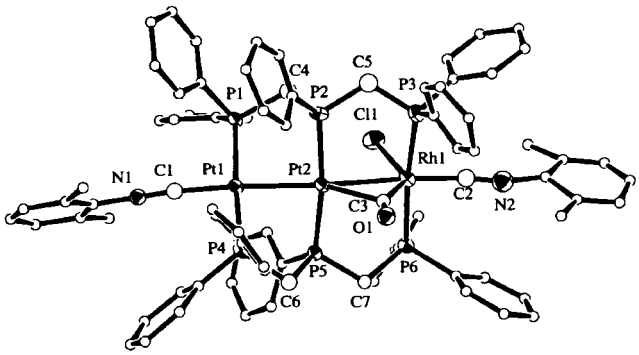

Figure 5. ORTEP plot of the complex cation of **10a**, $[Pt_2\{RhCl(\mu\text{-CO})(XylNC)\}(\mu\text{-dpmp})_2(XylNC)]^{2+}$. Carbon atoms of the phenyl and xylyl groups are drawn with arbitrary circles, and hydrogen atoms are omitted for clarity.

Table 8. Selected Bond Distances (Å) and Angles (deg) for $[Pt_2\{RhCl(\mu\text{-CO})(XylNC)\}(\mu\text{-dpmp})_2(XylNC)](PF_6)_2$ (10a)[a]

Bond Distances			
Pt(1)−Pt(2)	2.667(1)	Pt(1)−P(1)	2.307(6)
Pt(1)−P(4)	2.326(6)	Pt(1)−C(1)	1.94(2)
Pt(2)−Rh(1)	2.762(2)	Pt(2)−P(2)	2.297(6)
Pt(2)−P(5)	2.256(6)	Pt(2)−C(3)	2.16(2)
Rh(1)−Cl(1)	2.488(7)	Rh(1)−P(3)	2.315(7)
Rh(1)−P(6)	2.355(6)	Rh(1)−C(2)	1.84(2)
Rh(1)−C(3)	1.90(2)	O(1)−C(3)	1.18(2)
N(1)−C(1)	1.19(3)	N(1)−C(11)	1.43(3)
N(2)−C(2)	1.15(3)	N(2)−C(21)	1.39(4)
Bond Angles			
Pt(2)−Pt(1)−P(1)	90.6(2)	Pt(2)−Pt(1)−P(4)	86.5(2)
Pt(2)−Pt(1)−C(1)	176.3(6)	P(1)−Pt(1)−P(4)	174.3(2)
P(1)−Pt(1)−C(1)	92.1(6)	P(4)−Pt(1)−C(1)	91.1(6)
Pt(1)−Pt(2)−Rh(1)	163.85(5)	Pt(1)−Pt(2)−P(2)	88.1(2)
Pt(1)−Pt(2)−P(5)	83.6(2)	Pt(1)−Pt(2)−C(3)	152.1(5)
Rh(1)−Pt(2)−P(2)	91.5(2)	Rh(1)−Pt(2)−P(5)	94.6(2)
Rh(1)−Pt(2)−C(3)	43.4(5)	P(2)−Pt(2)−P(5)	169.1(2)
P(2)−Pt(2)−C(3)	101.5(5)	P(5)−Pt(2)−C(3)	89.1(5)
Pt(2)−Rh(1)−Cl(1)	79.6(2)	Pt(2)−Rh(1)−P(3)	93.4(2)
Pt(2)−Rh(1)−P(6)	92.0(2)	Pt(2)−Rh(1)−C(2)	168.7(7)
Pt(2)−Rh(1)−C(3)	51.2(6)	Cl(1)−Rh(1)−P(3)	87.5(2)
Cl(1)−Rh(1)−P(6)	95.7(2)	Cl(1)−Rh(1)−C(2)	111.5(7)
Cl(1)−Rh(1)−C(3)	130.5(6)	P(3)−Rh(1)−P(6)	174.1(2)
P(3)−Rh(1)−C(2)	85.3(8)	P(3)−Rh(1)−C(3)	90.2(6)
P(6)−Rh(1)−C(2)	89.0(8)	P(6)−Rh(1)−C(3)	91.5(6)
C(2)−Rh(1)−C(3)	117.5(9)		
C(1)−N(1)−C(11)	173(2)	C(2)−N(2)−C(21)	161(3)
Pt(1)−C(1)−N(1)	168(2)	Rh(1)−C(2)−N(2)	173(2)
Pt(2)−C(3)−Rh(1)	85.4(8)	Pt(2)−C(3)−O(1)	123(2)
Rh(1)−C(3)−O(1)	152(2)		

[a] Estimated standard deviations are given in parentheses.

observed at 1853 cm^{-1} in a CH_2Cl_2 solution). The former bands are very close to those of **6a**, and the latter falls between the ranges for terminal and bridging carbonyl groups. The $^{31}P\{^1H\}$ NMR spectrum of **10a** was not dramatically changed from that of **6a**, suggesting that the linear $\{Pt_2Rh(\mu\text{-dpmp})_2\}$ core of **6a** was retained during the reaction. The $^{13}C\{^1H\}$ NMR spectrum of **10a** prepared with ^{13}C-enriched CO exhibited one doublet for the carbonyl carbon at δ 205.0 ppm due to coupling to the Rh atom (J_{RhC} = 60 Hz), which was accompanied by two sets of ^{195}Pt satellite peaks (J_{PtC} = 356 and 137 Hz).

The detailed structure of **10a** was determined by an X-ray crystallographic analysis (Figure 5 and Table 8). The linear trimetallic framework $\{Pt_2Rh(\mu\text{-dpmp})_2\}$ is essentially retained but is slightly bending with Pt(1)−

Scheme 5

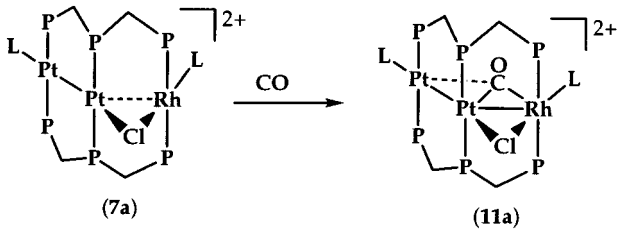

Scheme 6

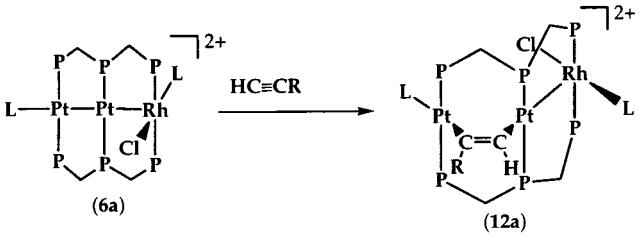

Pt(2)−Rh(1) = 163.85(5)°. One carbonyl group is incorporated into the cluster and asymmetrically bridges the Rh(1) and Pt(2) atoms (Rh(1)−C(3)−Pt(2) = 85.4(8)°). The C(3)−O(1) bond length is 1.18(2) Å. The Rh(1)−C(3) distance of 1.90(2) Å is considerably shorter than the Pt(2)−C(3) lengths of 2.16(2) Å, and the Rh(1)−C(3)−O(1) angle of 152(2)° is larger than the Pt(2)−C(3)−O(1) angle of 123(2)°. These CO bridging structures can be regarded as a semibridging mode, as observed in $[PtRhCl_2(\mu\text{-}CO)(\mu\text{-}dppm)_2]^+$ [32] $[[Rh_2(CO)_2(\mu\text{-}CO)(\mu\text{-}dppm)_2]$,[33] and $[RhIr(CH_3)(CO)(\mu\text{-}CO)(\mu\text{-}dppm)_2]^+$,[34] in which the carbonyl group interacts more strongly with the Rh atom than with the Pt one. Even upon the addition of CO between the Pt and Rh atoms, the Pt(2)−Rh(1) distance of 2.762(2) Å exhibits just a slight increase from that of the starting complex **6a** (2.7537(5) Å), indicative of a Pt−Rh single bond. The geometry of the Rh center is best described as a trigonal bipyramidal structure when the metal−metal bond is excluded; the two P atoms occupy the apical positions (P(3)−Rh(1)−P(6) = 174.1(2)°) and the CO, RNC, and Cl ligands comprise the equatorial triangular plane (Cl(1)−Rh(1)−C(2) = 111.5(7)°, Cl(1)−Rh(1)−C(3) = 130.5(6)°, and C(2)−Rh(1)−C(3) = 117.5(9)°). There is no bonding interaction between the Pt(2) and Cl(1) atoms on the basis of their interatomic distance (3.366(6) Å).

The asymmetrical A-frame cluster **7a** also reacted with CO (1 atm) to afford the yellow complex $[Pt_2\{Rh(\mu\text{-}Cl)(\mu\text{-}CO)(XylNC)\}(\mu\text{-}dpmp)_2(XylNC)](PF_6)_2$ (**11a**) in good yield (Scheme 5). Complex **11a** was fairly stable in solution and did not restore the starting cluster **7a** by bubbling N_2 into the solution. The elemental analysis indicated that complex **11a** is a 1:1 adduct of **7a** and CO, and the IR spectrum showed the presence of two kinds of terminal isocyanide ligands at 2162 and 2124 cm^{-1} and a carbonyl group at 1818 cm^{-1}. The CO stretching frequency in **11a** is lower by ca. 20 cm^{-1} than in **10a**. The $^{31}P\{^1H\}$ NMR spectral pattern is almost identical to that of **7a**, whereas the one-bond coupling to Rh in **11a** ($^1J_{RhP}$ = 95 Hz) is smaller than that in **7a** (122 Hz). In the $^{13}C\{^1H\}$ NMR spectrum of **11a** prepared with ^{13}C-enriched CO, one doublet for the carbonyl carbon was observed at δ 212.2 ppm (J_{RhC} = 36 Hz) accompanied by two sets of ^{195}Pt satellite peaks (J_{PtC} = 515 and 246 Hz). The value of $^1J_{RhC}$ is typical of a bridging carbonyl.[31] In comparison with the ^{13}C NMR spectral parameters for the carbonyl carbon of **10a**, the resonance in **11a** was downfield shifted by ∼7 ppm with a smaller coupling constant with the Rh atom and larger ones with the Pt centers. These spectral features suggested that the pseudo-C_s symmetrical cluster core of $\{Pt_2Rh(\mu\text{-}dpmp)_2\}$ was retained during the reaction and the trapped CO interacted more strongly with Pt and weakly with Rh, respectively, when compared with **10a**. Molar conductivity measurements suggested that cluster **11a** (292 S cm^2 mol^{-1}) is a 1:2 electrolyte like **6a** (273 S cm^2 mol^{-1}). From these, an estimated structure of **11a** is illustrated in Scheme 5, where a CO molecule is trapped into the backside pocket of the Pt(μ-Cl)Rh A-frame. The similar reaction has been observed with the Pt(μ-Cl)Rh and Rh(μ-Cl)Rh dinuclear complexes.[26,32,34,35]

Reactions of 6a with Activated Alkyne. When complex **6a** was reacted with the electron-deficient terminal alkyne HC≡CCO_2Me at reflux in CH_2Cl_2, red crystals formulated as $[Pt_2\{RhCl(XylNC)\}(\mu\text{-}dpmp)_2(\mu\text{-}HCCCO_2Me)(XylNC)](PF_6)_2$ (**12a**) were obtained in 38% yield. The internal alkynes such as $RO_2CC{\equiv}CCO_2R$ (R = Me, Et) did not react with **6a**. The IR spectrum showed the C═O (1688 cm^{-1}) and C═C (1557 cm^{-1}) stretching bands as well as a broad band around 2130 cm^{-1} for the terminal isocyanide ligands, which were similar to those of $[Pt_3(\mu\text{-}dpmp)_2(\mu\text{-}HC{=}CCO_2Me)(XylNC)_2]^{2+}$ derived from the reaction of *linear*-$[Pt_3(\mu\text{-}dpmp)_2(XylNC)_2]^{2+}$ (**2a**) with HC≡CCO_2Me.[8] The ^1H NMR spectrum indicated the presence of XylNC, HC_2CO_2Me, and dpmp with a 2:1:2 ratio. In the $^{31}P\{^1H\}$ NMR spectrum, the spectral patterns for the P atoms bound to the Rh center did not largely change from those in **6a**; the *trans*-coupled AA′ multiplets (δ 26.4 and 5.9 ppm with $^2J_{PP'}$ = 438 Hz) are further split into doublets due to coupling to Rh ($^1J_{RhP}$ = 88 and 89 Hz). In contrast, the peaks for the Pt-bound P atoms were eventually altered to a complicated BB′CC′ pattern around 2 to −15 ppm, although the spectral parameters were not resolved. These spectral features implied that the alkyne molecule reacted with the Pt_2 unit rather than the Rh center. By analogy with the structures of $[Pt_3(\mu\text{-}dpmp)_2(\mu\text{-}HC{=}CCO_2Me)(XylNC)_2]^{2+}$ [8] and $[Rh_2Pd(CO)_2(\mu\text{-}Cl)Cl_2(\mu\text{-}dpma)_2]^+$,[29] we speculated the structure of **12a** as depicted in Scheme 6. The alkyne was estimated to be inserted site-selectively into the Pt−Pt bond to form the asymmetrical A-frame cluster core, and the terminal alkyne carbon is expected to attach to the central Pt atom regioselectivly owing to steric factors.

Conclusions

The present study reports a synthetic route to new Pt−Pt−M (M = Rh, Ir) heterotrimetallic clusters with

(32) Xu, C.; Anderson, G. K.; Rath, N. P. *Inorg. Chim. Acta* **1997**, *265*, 241.
(33) Woodcock, C.; Eisenberg, R. *Inorg. Chem.* **1985**, *24*, 1287.
(34) Oke, O.; McDonald, R.; Cowie, M. *Organometallics* **1999**, *18*, 1629.
(35) Cowie, M. *Inorg. Chem.* **1979**, *18*, 286.

$d^9-d^9-d^8$ metal combination, the T-shaped linear clusters **6**, $[Pt_2\{MClL\}(\mu\text{-dpmp})_2L]^{2+}$, and the asymmetrical A-frame clusters **7**, $[Pt_2\{M(\mu\text{-Cl})L\}(\mu\text{-dpmp})_2L]^{2+}$ (L = XylNC). In particular, the coordinatively unsaturated 3:2:4 type clusters **6** with 44 valence electrons are interesting concerning their reactivity, and the linearly ordered Pt_2M structures with Pt−Pt covalent and Pt←M dative bonds are unprecedented, whereas Liu et al. recently reported the linear Os_3 cluster containing tandem metal−metal dative bonds.[36] Complex **6** reacted with isocyanide molecules to afford the linearly ordered 3:2:5 type clusters $[Pt_2\{MXL_2\}(\mu\text{-dpmp})_2L]^{n+}$ (**8a**, M = Rh, L = XylNC, X = Cl, n = 2; **9a**, M = Rh, L = X = XylNC, n = 3; **9b**, M = Ir, L = X = MesNC, n = 3). In complexes **8** and **9**, the added isocyanide molecules were attached exclusively to the group 9 metal ion to generate a coordinatively saturated metal center with 18 valence electron. Complex **6a** has a reversible binding property toward CO; the trapped CO acts as a semibridging unit between the Rh and Pt atoms to yield the linear $[Pt_2\{RhCl(\mu\text{-CO})L\}(\mu\text{-dpmp})_2L]^{2+}$ (**10a**: L = XylNC). The relatively inflexible linearly extended $\{Pt_2Rh(\mu\text{-dpmp})_2\}$ framework is assumed to be responsible for the efficient reversibility of the CO incorporation. In contrast, the electron-deficient terminal alkyne HC≡CCO_2R is inserted site-selectively into the Pt−Pt covalent bond versus the Pt←Rh dative bond, resulting in the $[Pt_2\{RhClL\}(\mu\text{-HC=CCO}_2R)(\mu\text{-dpmp})_2L]^{2+}$ (**12a**: R = Me, L = XylNC). These reactions clearly revealed that the reactive part of the linear heterotrimetallic Pt_2Rh core is altered depending on the nature of the substrate organic small molecules. The Rh center in **6a** is electron-deficient and acts as an electrophilic part, and the Pt_2 unit acts as a nucleophilic part by using the metal−metal-bonding electrons. These results could provide useful information in developing catalytic reactions by using mixed-metal cluster catalysts.

Acknowledgment. This work was partially supported by a Grant-in-Aid for Scientific Research from the Ministry of Education of Japan.

Supporting Information Available: Tabulations of crystallographic data, positional and thermal parameters, and bond lengths and angles of non-hydrogen atoms for **6a**, **6b**, **7a**, **8a**, **9b**, and **10a**. This material is available free of charge via the Internet at http://pubs.acs.org.

OM000843Z

(36) Liu, Y.; Leong, W. K.; Pomeroy, R. K. *Organometallics* **1998**, *17*, 3387.